



# LUND UNIVERSITY

## Retrieval of daily gross primary production over Europe and Africa from an ensemble of SEVIRI/MSG products

Martínez, B.; Sanchez-Ruiz, S.; Gilabert, M. A.; Moreno, A.; Campos-Taberner, M.; García-Haro, F. J.; Trigo, I. F.; Aurela, M.; Brümmer, C.; Carrara, A.; De Ligne, A.; Gianelle, D.; Grünwald, T.; Limousin, J. M.; Lohila, A.; Mammarella, I.; Sottocornola, M.; Steinbrecher, R.; Tagesson, T.

*Published in:*

International Journal of Applied Earth Observation and Geoinformation

*DOI:*

[10.1016/j.jag.2017.10.011](https://doi.org/10.1016/j.jag.2017.10.011)

2018

*Document Version:*

Peer reviewed version (aka post-print)

[Link to publication](#)

*Citation for published version (APA):*

Martínez, B., Sanchez-Ruiz, S., Gilabert, M. A., Moreno, A., Campos-Taberner, M., García-Haro, F. J., Trigo, I. F., Aurela, M., Brümmer, C., Carrara, A., De Ligne, A., Gianelle, D., Grünwald, T., Limousin, J. M., Lohila, A., Mammarella, I., Sottocornola, M., Steinbrecher, R., & Tagesson, T. (2018). Retrieval of daily gross primary production over Europe and Africa from an ensemble of SEVIRI/MSG products. *International Journal of Applied Earth Observation and Geoinformation*, 65, 124-136. <https://doi.org/10.1016/j.jag.2017.10.011>

*Total number of authors:*

19

*Creative Commons License:*

CC BY-NC-ND

### General rights

Unless other specific re-use rights are stated the following general rights apply:

Copyright and moral rights for the publications made accessible in the public portal are retained by the authors and/or other copyright owners and it is a condition of accessing publications that users recognise and abide by the legal requirements associated with these rights.

- Users may download and print one copy of any publication from the public portal for the purpose of private study or research.
- You may not further distribute the material or use it for any profit-making activity or commercial gain
- You may freely distribute the URL identifying the publication in the public portal

Read more about Creative commons licenses: <https://creativecommons.org/licenses/>

### Take down policy

If you believe that this document breaches copyright please contact us providing details, and we will remove access to the work immediately and investigate your claim.

LUND UNIVERSITY

PO Box 117  
221 00 Lund  
+46 46-222 00 00

Manuscript Number: JAG-D-17-00309R2

Title: Retrieval of daily gross primary production (GPP) over Europe and Africa from an ensemble of SEVIRI/MSG products

Article Type: Research Paper

Keywords: GPP, MSG, daily, water stress, light-use efficiency, LSA SAF.

Corresponding Author: Miss Beatriz Martinez,

Corresponding Author's Institution:

First Author: Beatriz Martinez

Order of Authors: Beatriz Martinez; Sergio Sánchez-Ruiz; M.Amparo Gilabert; Alvaro Moreno; Manuel Campos-Taberner; Javier F García-Haro; Isabel F Trigo; Mika Aurela; Christian Brümmer; Arnau Carrara; Anne De Ligne; Damiano Gianelle; Thomas Grünwald; Jean-Marc Limousin; Annalea Lohila; Ivan Mammarella; Matteo Sottocornola; Rainer Steinbrecher; Torbern Tagesson

Abstract: The main goal of this paper is to derive a method for a daily gross primary production (GPP) product over Europe and Africa taking the full advantage of the SEVIRI/MSG satellite products from the European Organization for the Exploitation of Meteorological Satellites (EUMETSAT) sensors delivered from the Satellite Application Facility for Land Surface Analysis (LSA SAF) system. Special attention is paid to model the daily GPP response from an optimized Monteith's light use efficiency model under dry conditions by controlling water shortage limitations from the actual evapotranspiration and the potential evapotranspiration (PET). The PET was parameterized using the mean daily air temperature at 2 m ( $T_a$ ) from ERA-Interim data. The GPP product (MSG GPP) was produced for 2012 and assessed by direct site-level comparison with GPP from eddy covariance data (EC GPP). MSG GPP presents relative bias errors lower than 40% for the most forest vegetation types with a high agreement ( $r > 0.7$ ) when compared with EC GPP. For drylands, MSG GPP reproduces the seasonal variations related to water limitation in a good agreement with site level GPP estimates (RMSE=2.11 g m<sup>-2</sup> day<sup>-1</sup>; MBE=-0.63 g m<sup>-2</sup> day<sup>-1</sup>), especially for the dry season. A consistency analysis against other GPP satellite products (MOD17A2 and FLUXCOM) reveals a high consistency among products (RMSD < 1.5 g m<sup>-2</sup> day<sup>-1</sup>) over Europe, North and South Africa. The major GPP disagreement arises over moist biomes in central Africa (RMSD > 3.0 g m<sup>-2</sup> day<sup>-1</sup>) and over dry biomes with MSG GPP estimates lower than FLUXCOM (MBD up to -3.0 g C m<sup>-2</sup> day<sup>-1</sup>). This newly derived product has the potential for analysing spatial patterns and temporal dynamics of GPP at the MSG spatial resolutions on a daily basis allowing to better capture the GPP dynamics and magnitude.

Opposed Reviewers:

## Retrieval of daily gross primary production over Europe and Africa from an ensemble of SEVIRI/MSG products

Martínez<sup>1\*</sup>, B., Sanchez-Ruiz<sup>1</sup>, S., Gilabert<sup>1</sup>, M.A., Moreno<sup>2</sup>, A., Campos-Taberner<sup>1</sup>, M., García-Haro<sup>1</sup>. F.J., Trigo<sup>3</sup>, I.F., Aurela<sup>4</sup>, M., Brümmer<sup>5</sup>, C., Carrara<sup>6</sup>, A., De Ligne<sup>7</sup>, A., Gianelle<sup>8</sup>, D., Grünwald<sup>9</sup>, T., Limousin<sup>10</sup>, J.M., Lohila<sup>11</sup>, A., Mammarella<sup>12</sup>, I., Sottocornola<sup>13</sup>, M., Steinbrecher<sup>14</sup>, R., Tagesson<sup>15,16</sup>, T.

- 1) Departament de Física de la Terra i Termodinàmica, Facultat de Física, Universitat de València, Burjassot, Spain.
- 2) Numerical Terradynamic Simulation Group, University of Montana, Missoula, MT, USA.
- 3) Instituto Português do Mar e da Atmosfera (IPMA), Lisbon, Portugal.  
(FLUXNET EC IP)
- 4) Finnish Meteorological Institute, Helsinki, Finland.
- 5) Thünen Institute of Climate-Smart Agriculture, Braunschweig, Germany.
- 6) Fundación Centro de Estudios Ambientales del Mediterráneo (CEAM), Paterna, Spain.
- 7) TERRA Teaching and Research Centre, Gembloux Agro-Bio Tech, University of Liege, Gembloux, Belgium.
- 8) Department of Sustainable Agro-Ecosystems and Bioresources, Research and Innovation Center, Fondazione Edmund Mach, Michele all' Adige Trento, Italy.
- 9) Technische Universität Dresden, Institute of Hydrology and Meteorology, Tharandt, Germany.
- 10) Centre d'Ecologie Fonctionnelle et Evolutive CEFE, UMR 5175, CNRS - Université de Montpellier - Université Paul Valéry Montpellier - EPHE, Montpellier, France.
- 11) Finnish Meteorological Institute, Helsinki, Finland.
- 12) Department of Physics, University of Helsinki, Helsinki, Finland.
- 13) Department of Science, Waterford Institute of Technology, Waterford, Ireland.
- 14) Department of Atmospheric Environmental Research, Karlsruhe Institute of Technology, Institute of Meteorology and Climate Research (KIT/IMK-IFU), Garmisch-Partenkirchen, Germany.
- 15) Department of Physical Geography and Ecosystem Sciences, Lund University, Lund, Sweden.
- 16) Department of Geosciences and Natural Resource Management (IGN), University of Copenhagen, Copenhagen, Denmark.

(\* ) Corresponding author:

E-mail address: [beatriz.martinez@uv.es](mailto:beatriz.martinez@uv.es)

Phone: +34 96 3543113; fax: +34 96 3543385.

## 1 **ABSTRACT**

2 The main goal of this paper is to derive a method for a daily gross primary production (GPP) product  
3 over Europe and Africa taking the full advantage of the SEVIRI/MSG satellite products from the  
4 European Organization for the Exploitation of Meteorological Satellites (EUMETSAT) sensors  
5 delivered from the Satellite Application Facility for Land Surface Analysis (LSA SAF) system. Special  
6 attention is paid to model the daily GPP response from an optimized Monteith's light use efficiency  
7 model under dry conditions by controlling water shortage limitations from the actual  
8 evapotranspiration and the potential evapotranspiration (PET). The PET was parameterized using the  
9 mean daily air temperature at 2 m ( $T_a$ ) from ERA-Interim data. The GPP product (MSG GPP) was  
10 produced for 2012 and assessed by direct site-level comparison with GPP from eddy covariance data  
11 (EC GPP). MSG GPP presents relative bias errors lower than 40% for the most forest vegetation types  
12 with a high agreement ( $r > 0.7$ ) when compared with EC GPP. For drylands, MSG GPP reproduces the  
13 seasonal variations related to water limitation in a good agreement with site level GPP estimates  
14 ( $RMSE = 2.11 \text{ g m}^{-2} \text{ day}^{-1}$ ;  $MBE = -0.63 \text{ g m}^{-2} \text{ day}^{-1}$ ), especially for the dry season. A consistency analysis  
15 against other GPP satellite products (MOD17A2 and FLUXCOM) reveals a high consistency among  
16 products ( $RMSD < 1.5 \text{ g m}^{-2} \text{ day}^{-1}$ ) over Europe, North and South Africa. The major GPP disagreement  
17 arises over moist biomes in central Africa ( $RMSD > 3.0 \text{ g m}^{-2} \text{ day}^{-1}$ ) and over dry biomes with MSG  
18 GPP estimates lower than FLUXCOM (MBD up to  $-3.0 \text{ g C m}^{-2} \text{ day}^{-1}$ ). This newly derived product has  
19 the potential for analysing spatial patterns and temporal dynamics of GPP at the MSG spatial  
20 resolutions on a daily basis allowing to better capture the GPP dynamics and magnitude.

21 Keywords: GPP, MSG, daily, water stress, light-use efficiency, LSA SAF.

## 22 **1. Introduction**

23 Serious concerns associated with climate change are strongly present on the African and European  
24 continents leading, among others, to significant effects on plant distribution, growth and productivity  
25 (EEA, 2012; IPCC, 2014). Thus, a better understanding of the productivity dynamics of ecosystems  
26 across these continents is needed.

27 Terrestrial ecosystem models provide a powerful tool to integrate our understanding on ecosystem  
28 functioning and observations at multiple scales in response to multiple environmental factors (Zhao  
29 et al., 2005; Tian et al., 2010; Yebra et al., 2015). There is a renewed interest in developing carbon  
30 flux models that are entirely driven by remotely sensed (RS) observations to estimate gross primary  
31 production (GPP) (Running et al., 2004; Gilabert et al., 2015; Tramontana et al., 2016). Estimates of  
32 daily GPP (MOD17) (Heinsch et al., 2006; Zhao et al., 2011; Running et al., 2015) are produced

1 operationally for the global terrestrial surface using imagery from the MODerate resolution Imaging  
2 Spectroradiometer (MODIS) sensor (Running et al., 2004). Additionally, there clearly is a motivation  
3 to extend knowledge acquired from modeling efforts with the MODIS datasets to other sensor's  
4 data, such as the Spinning Enhanced Visible and InfraRed Imager (SEVIRI) on board of the Meteosat  
5 Second Generation (MSG) platform.

6 Most of the methodologies for the estimation of GPP from satellite data, such as the widely used  
7 MODIS GPP product (Zhao et al., 2011), rely on the well-known satellite-based Production Efficiency  
8 Models (PEMs). Most of the PEMs are based on Monteith's light use efficiency (LUE) concept  
9 (Monteith, 1972). This concept is still considered to be efficient and widely applicable for the  
10 prediction of GPP at different spatial and temporal scales (Waring and Running, 2007) and considers  
11 GPP equal to the product of the incoming photosynthetically active radiation (PAR), the fractional  
12 absorption of that flux ( $f_{APAR}$ ) and the light use efficiency ( $\epsilon$ ). The latter can be operationally  
13 parameterized as a function of a maximum value ( $\epsilon_{max}$ ), which is reduced by different factors related  
14 with types of stress that affect the functionality of the plant, such as water availability and thermal  
15 stress. These factors range from 0 (total inhibition) to 1 (no inhibition).  $\epsilon_{max}$  can be set as invariant  
16 across sites and biomes (Myneni et al., 1995) or be derived from biome-dependent values (Garbulsky  
17 et al., 2010). According to Schaefer et al. (2012), three areas of the PEMs still need improvements: 1)  
18 parameterization of  $\epsilon_{max}$ , 2) response function under low temperatures, and 3) GPP response under  
19 dry conditions (mainly driven by water stress factors).

20 In particular, the MODIS standard product parameterizes  $\epsilon$  as the product of a biome-specific  $\epsilon_{max}$   
21 and the thermal and the water stress factors, which depend on minimum air temperature and vapor  
22 pressure deficit, respectively (Zhao et al., 2011; Heinsch et al., 2006). Another parameterization of  
23 the water stress based on a water stress coefficient ( $C_{ws}$ ) has been applied successfully to derive daily  
24 GPP estimates in Mediterranean ecosystems (Maselli et al., 2009; Gilabert et al., 2015; Sánchez-Ruiz  
25 et al., 2017).  $C_{ws}$  accounts for the limited photosynthetic activity in case of short-term water stress  
26 from a simplified local water budget based on the ratio of actual evapotranspiration (AET) and  
27 potential evapotranspiration (PET). Commonly, evapotranspiration (ET) is normalized by the  
28 reference evapotranspiration or by PET in order to characterize water stress (Sepulcre et al., 2014).  
29 PET is driven by available energy, while AET reflects an immediate response of vegetation  
30 productivity to water-storage (Fisher et al., 2011). Different approaches have been proposed to  
31 account for the water stress by means of the AET and PET (Sepulcre et al., 2014; Idso et al., 1981).

32 The main goal of this paper is to provide a method for the estimation of daily GPP over Europe and  
33 Africa from the integration of an ensemble of SEVIRI/MSG products into an optimized LUE model that

1 accounts for water shortage limitations. SEVIRI/MSG satellite products from the European  
2 Organization for the Exploitation of Meteorological Satellites (EUMETSAT) sensors delivered from the  
3 Satellite Application Facility for Land Surface Analysis (LSA SAF) system are used ([http://lsa-  
5 saf.eumetsat.int](http://lsa-<br/>4 saf.eumetsat.int)) for 2012. This year is selected due to the unavailability of the necessary inputs for  
6 other years. The used set of LSA-SAF products derived from SEVIRI/MSG offers convenient spatial  
7 coverage (Europe, Africa and parts of South America) and resolution (Trigo et al., 2011). Moreover,  
8 these products are produced operationally in near-real time with generation rates varying from 30  
9 min in the case of ET to daily or 10-day in the case of several vegetation parameters, which makes  
10 them particularly suitable for the development of early warning procedures such as drought  
11 prediction. Since water availability and radiation are known as main potential climatic constraints to  
12 vegetation productivity in many areas of Europe and Africa (Nemani et al., 2003), special attention is  
13 paid to capture the GPP response under dry conditions by controlling the water shortage limitations.  
14 Thus, a water stress coefficient ( $C_{ws}$ ) based on the ratio between AET and PET, with PET  
parameterized using Jensen & Haise (1965), is proposed.

15 The use of the MSG GPP product can benefit from different aspects. 1) The high quality of the daily  
16 down-welling radiation flux (DIDSSF) product (bias and mean absolute error below 6%) confers the  
17 MSG GPP estimates of a high reliability. The DIDSSF product is used to compute both the PAR and the  
18  $C_{ws}$ , being the PAR the most influential variable in the GPP variance (e.g. over 60% of the variance  
19 was explained by the PAR in forests over Spain (Gilbert et al., 2015)). 2) The daily basis of the MSG  
20 GPP product aids, among others, a better characterization of vegetation state and temporal  
21 processes (e.g. sudden changes from natural hazards or management practices). 3) Clouds effect on  
22 the  $f_{APAR}$  and DIDSSF is better sampled at daily temporal scale allowing a more accurate  
23 characterization as compared to the MODIS product (Heinsch et al., 2006; Gilbert et al., 2015) and  
24 also a better understanding of the cloud coverage on the carbon uptake by vegetation.

25 The performance of the resulting GPP product (MSG GPP) is assessed by site-level comparisons using  
26 GPP estimates from eddy covariance (EC) towers. Moreover, the MSG GPP assessment includes  
27 consistency analyses against alternative GPP products available from independent remote sensing  
28 global data, such as MODIS GPP (MOD17A2) and global flux fields from the Max Planck Institute  
29 (MPI) (FLUXCOM) products. The paper first introduces the theoretical basis for the daily GPP retrieval  
30 together with the description of the required inputs. The next section describes the MSG GPP  
31 assessment and the data used for this purpose. It is followed by a presentation of the obtained  
32 results and a discussion section reporting on the differences, advantages and limitations of the MSG  
33 GPP retrievals. The main conclusions are presented in the final section.

## 1 2. Daily GPP retrieval

2 The methodology used to derive daily GPP ( $\text{g m}^{-2} \text{day}^{-1}$ ) was based on Monteith's LUE approach:

$$3 \quad \text{GPP} = \varepsilon f_{\text{APAR}} \text{PAR} \quad (1)$$

4 where

$$5 \quad \varepsilon = \varepsilon_{\text{max}} C_{\text{ws}}. \quad (2)$$

6 Parameter  $\varepsilon$  was parameterized as  $\varepsilon_{\text{max}}$  downregulated by the water stress coefficient ( $C_{\text{ws}}$ ). Overall,  
7 optimized  $\varepsilon_{\text{max}}$  values can range between 0.55–3.5  $\text{g MJ}^{-1}$ , as reported by several authors (Garbulsy  
8 et al., 2010; Sjöström et al., 2013; Tagesson et al., 2015). Three values were assigned to the main  
9 ecosystems types: 1.8  $\text{g MJ}^{-1}$  for deciduous broadleaf forest (DBF), 1.5  $\text{g MJ}^{-1}$  for evergreen needleleaf  
10 forest (ENF), and 1.2  $\text{g MJ}^{-1}$  for remaining ecosystem types (Garbulsy et al., 2010). GPP was not  
11 computed for desert areas due to the lack of values for some inputs (e.g. DMET) and the high error  
12 provided by the  $f_{\text{APAR}}$  product in these areas.

13  $C_{\text{ws}}$  was parameterized using a variant of the formulation proposed by Maselli et al. (2009):

$$14 \quad C_{\text{ws}} = 0.6 + 0.4 \frac{\text{AET}}{\text{PET}}. \quad (3)$$

15 Thus,  $C_{\text{ws}}$  can vary between 0.6 (when water shortage reduces photosynthesis to 60 % of its potential  
16 value) and 1.0 (when there is no such reduction). This  $C_{\text{ws}}$  is not as restrictive as the one proposed for  
17 Mediterranean ecosystems by Masselli et al. (2009, 2013), in order to reach a compromise between  
18 the ability to cope with water limitation during the dry season and the ability to grow at high rates  
19 under more favorable water conditions. PET ( $\text{mm day}^{-1}$ ) was parameterized using the Jensen-Haise  
20 (JS) empirical equation (Jensen & Haise, 1965):

$$21 \quad \text{PET} = \frac{R_g(0.025T_a + 0.08)}{2450}. \quad (4)$$

22 Where  $R_g$  refers to the daily global irradiation ( $\text{kJ m}^{-2} \text{day}^{-1}$ ) and  $T_a$  is the daily averaged near-surface  
23 air temperature in  $^{\circ}\text{C}$ .

24 The JS method (Eq. 4) requires only information on climate or meteorological drivers; an important  
25 aspect when applying the model on large region scales. The JS approach was originally derived for  
26 the semi-arid parts of the United States but is currently used across different climate zones and  
27 biomes at the North Dakota Agricultural Weather Network (NDAWN, <http://ndawn.ndsu.nodak.edu/>)

1 for estimating potential evapotranspiration. It was also successfully applied at regional level over  
2 Spain and Italy using MODIS and SPOT-VGT data along with meteorological data to derive an  
3 optimized GPP product that accounted for water stress (Maselli et al., 2009; Gilabert et al., 2015).

4 A subsequent analysis of different water stress parameterizations at EC flux towers in Spain indicated  
5 the JS as one of the best methods, explaining 31% and 48% of  $\varepsilon$  variance in open shrublands and  
6 savanna, respectively (Sánchez-Ruiz et al., 2017). The JS approach was also evaluated for two very  
7 different sites (one semi-arid savanna grassland and one boreal forest) in the present study,  
8 indicating reasonable PET and CWS estimates across various biomes (Fig S1 in supplementary  
9 material).

10 The input variables required for the GPP retrieval by means of Eq. 1 are described as follows.

## 11 **2.1 PAR**

12 PAR is the photosynthetically active radiation in the 0.4–0.7  $\mu\text{m}$  spectral range and was computed as  
13 the 46% of daily irradiation (Iqbal, 1983). Daily irradiation images for Europe and Africa provided  
14 from the daily down-welling radiation flux (DIDSSF) MSG product (LSA-201) at 3–5 km (depending on  
15 the latitude and the distance to nadir view) were used. The DIDSSF product essentially depends on  
16 the solar zenith angle, on cloud coverage and, to a lesser extent, on atmospheric absorption and  
17 surface albedo (LSA SAF, 2012; Geiger et al., 2008). It is computed by integrating the downward  
18 surface solar flux (DSSF) product every 30 minutes over a whole day. A validation of DSSF using *in situ*  
19 data from six European ground measurement stations throughout two years was performed by  
20 Geiger et al. (2008). Results show a difference between instantaneous satellite estimates and ground  
21 measurements of about 40 and 110  $\text{W m}^{-2}$  for clear and cloudy sky conditions, respectively. A more  
22 thorough validation of the MSG DSSF product was carried out in Spain (Moreno et al., 2013). The  
23 resulting statistics from this validation show a bias of  $-0.12 \text{ MJ m}^{-2}$  (rMBD of about 1%) and a mean  
24 absolute difference of  $1.0 \text{ MJ m}^{-2}$  (rMAD of 6%) in terms of daily global irradiation.

## 25 **2.2. $f_{\text{APAR}}$**

26  $f_{\text{APAR}}$  is the fraction of PAR that is absorbed by leaves and provides a link between the canopy  
27 function, i.e. its energy absorption capacity, and its structure and condition. The MSG  $f_{\text{APAR}}$  product  
28 (MDFAPAR, LSA-407) delivered by the LSA SAF network was used as input. It has a 3.1 km spatial  
29 resolution (sub-satellite point) and daily frequency over the geostationary MSG grid (García-Haro et  
30 al., 2015). The MDFAPAR product is based on a linear relationship between the Renormalized  
31 Difference Vegetation Index (RDVI), computed from clear-sky top of the canopy reflectances in the

1 red ( $R_R$ ) and near infrared ( $R_{NIR}$ ) bands for an optimal angular geometry in the solar principal plane  
2 (Roujean and Bréon, 1995). It was reported that the MSG  $f_{APAR}$  deviated from the other  $f_{APAR}$  products  
3 in the order of 0.1 (García-Haro et al., 2015).

4 In this study, the  $f_{APAR}$  time series were filtered and reconstructed using an optimized LOcally  
5 WEighted regression and Smoothing Scatterplots (LOWESS) method (Moreno et al., 2014; Gilabert et  
6 al., 2015), which captures the upper envelope of the time-series, interpolates the missing data and  
7 removes most of the noise of the original unfiltered signal. The LOESS approach is recommended in  
8 most remote sensing applications, such as gap-filling, cloud-replacement, and observing temporal  
9 dynamics *in situ* where rapid seasonal changes are produced (Moreno et al., 2014).

### 10 **2.3 $C_{ws}$**

11 The daily  $C_{ws}$  was computed using the daily AET LSA SAF product (DMET, LSA-302) and the daily PET  
12 derived from the JS parameterization (Eq. 4). Equation 4 uses two inputs of the LSA SAF system: the  
13 DIDSSF operational product and the daily mean  $T_a$  at SEVIRI/MSG disk (LSA SAF, 2016a). The  $T_a$  MSG  
14 product is derived from the interpolation of ERA-Interim data produced by the European Centre for  
15 Medium-Range Weather Forecasts (ECMWF, <http://apps.ecmwf.int/datasets/>), originally at  $0.75^\circ \times$   
16  $0.75^\circ$ . The data are then interpolated to SEVIRI pixel scale by a bi-linearly interpolation method. The  
17 temperature fields are further adjusted to correct for the differences between ERA-Interim surface  
18 orography and pixel height, assuming a constant lapse rate of  $0.67^\circ\text{C}/100\text{m}$ . The interpolation  
19 procedure is designed to minimize the impact of model resolution.

20 DMET matches observed variations with a high compromise (i.e. product requirement criterion  
21 satisfied to a rate higher than 70% in most of the validation sites) for well-watered sites and an  
22 expected seasonal variation for temperate forests. It is also highly correlated with spatial variability  
23 in ECMWF daily-accumulated ET (correlation values from 0.85 to 0.95) (LSA SAF, 2010). However, the  
24 DMET product is underestimated globally in comparison with the ECMWF one, especially in Africa  
25 and South America (LSA SAF, 2010).

### 26 **3. Data for MSG GPP assessment**

27 The daily MSG GPP performance and assessment include: 1) qualitative evaluations of MSG GPP  
28 estimates in relation to characteristic spatial and seasonal patterns, 2) direct comparison of daily  
29 carbon flux estimates with *in situ* EC tower GPP estimations based on daily carbon flux  
30 measurements, and 3) consistency checking against other synergistic global carbon products. The  
31 data used for the proposed assessment are described below.

### 1 **3.1 GPP estimates from Eddy Covariance flux towers**

2 Daily GPP data from 18 EC flux towers were downloaded from the global Fluxes Database Cluster  
3 data set (FLUXNET). The FLUXNET2015 (<http://fluxnet.fluxdata.org/>) dataset consists of standardized  
4 and high quality data products collected from multiple regional EC flux networks (Valentini et al.,  
5 2014). The FLUXNET2015 GPP products were obtained applying standard flux-partitioning algorithms  
6 after the net ecosystem exchange time series were gap filled (Lasslop et al., 2010) and went through  
7 a rigorous QA/QC procedure (Pastorello et al., 2014). The model efficiency method reference GPP  
8 product (GPP\_DT\_VUT\_REF) (Kumar et al., 2016) calculated using daily data (Lasslop et al., 2010) was  
9 compared with the MSG GPP estimates.

10 However, such direct comparison requires that the surface characteristics (vegetation composition)  
11 of the pixel used for RS products and of the EC measurements footprint are similar. To solve this  
12 issue, the homogeneity of a 5 km × 5 km area surrounding the measurement tower was analyzed. For  
13 this purpose, the 1 km Global Land Cover 2000 (GLC2000) (Bartholomé and Belward, 2005) was used.  
14 The selection of adequate sites for comparing MSG GPP and EC estimates without bias due to surface  
15 spatial heterogeneity was based on the following steps, i) computation of the land cover percentages  
16 inside the 5 km × 5 km area (i.e. MSG pixel size over Europe) based on the GLC2000, ii) pre-selection  
17 of EC sites as those with two or less land cover classes within the 5 km × 5 km area and one land  
18 cover percentage greater than 80%, and iii) final selection of EC sites by visual inspection using  
19 Google Earth™ (Table 1). Figure 1 shows the GLC2000 geo-located to a standard SEVIRI grid. The  
20 selected EC sites are also included (red crosses). A generalized classification was obtained by  
21 aggregating several similar land cover classes from the 23-class GLC2000. The study area was thus  
22 described through a generalized thematic legend of 6 major land covers: evergreen broadleaf forest  
23 (7%), deciduous broadleaf forest (13%), evergreen needleleaf forest (2%), mixed forest (5%),  
24 shrublands (11%), grasslands (15%), croplands (15%) and bare soil (32%). This generalization reduces  
25 the number of classes while preserving the essence of the geographical patterns of the study area  
26 (Martínez et al., 2013).

27 [INSERT TABLE 1]

28 [INSERT FIGURE 1]

29

### 30 **3.2 MODIS GPP product (MOD17A2)**

1 The MODIS GPP 8-day product (MOD17A2 version-55) at 1 km was retrieved from the online Reverb,  
2 courtesy of the NASA EOSDIS Land Processes Distributed Active Archive Center (LP DAAC),  
3 USGS/Earth Resources Observation and Science (EROS) Center, (<https://reverb.echo.nasa.gov>).  
4 Version-55 is post-processed from the MODIS GPP version-5 dataset, in which contaminated MODIS  
5 FPAR/LAI inputs to the MOD15 algorithm have been cleaned (Zhao and Running, 2010). The MODIS  
6 products were reprojected to Geographic (WGS84) coordinate projection and geo-located to a  
7 standard SEVIRI grid in order to reproduce the characteristics of the MSG product. The reprojection  
8 step was performed by averaging all fine resolution pixel values of the MODIS product that overlap  
9 with a given SEVIRI pixel. Pixels identified as water, snow or unreliable values were excluded during  
10 the averaging process (García-Haro et al., 2008).

### 11 **3.3 FLUXCOM product**

12 The FLUXCOM product provides monthly spatio-temporal fields at  $0.5^\circ \times 0.5^\circ$  spatial resolution for  
13 the period 1980-2013 from a combination of machine learning (ML) algorithms trained on site-level  
14 EC GPP estimates ([www.fluxcom.org](http://www.fluxcom.org)). The FLUXCOM data are available from the Data Portal of the  
15 Max Planck Institute for Biogeochemistry ([www.bgc-jena.mpg.de/geodb/projects](http://www.bgc-jena.mpg.de/geodb/projects)). The GPP fields are  
16 generated by 3 machine learning (ML) methods, namely, random forest (RF), artificial neural  
17 networks (ANN), and multivariate adaptive regression splines (MARS). The three methods are forced  
18 with meteorological data and mean seasonal cycles of several MODIS based variables (RS+METEO  
19 setup) on EC sites belonging to the FLUXNET La Thuile synthesis data set and CarboAfrica network  
20 (Valentini et al., 2014; Tramontana et al., 2016; Jung et al. 2017).

21 In this work, the GPP derived from the ANN (Papale and Valentini, 2003), which utilizes the  
22 relationship among the micrometeorological variables, was used. The application of ANN techniques  
23 to carbon flux dynamics study for European forest ecosystem has been demonstrated by several  
24 authors (e.g. Van Wijk and Bouten, 1999; Papale and Valentini, 2003). The FLUXCOM data were  
25 reprojected to Geographic (WGS84) coordinate projection at 1 km and the geo-located to a standard  
26 SEVIRI grid by the same procedure as for the MODIS data.

## 27 **4. Results**

### 28 **4.1 Spatial and temporal MSG GPP patterns**

29 Figure 2 presents an overview of MSG GPP estimates showing one daily field every-two-months and  
30 covering a full year (2012). In general, maximum GPP values are observed in May-July in Europe and  
31 September-March in Africa (Figure 2). The northern latitudes experience low GPP during winter and

1 early spring due to prevalent cold temperatures and moderate radiation whereas GPP levels are high  
2 over the Equatorial belt throughout the whole year owing to relatively warm temperature, moist and  
3 radiation availability. GPP of semi-arid regions (e.g. South Spain, Sahel region, East Africa, South  
4 Africa) closely follows seasonality of rainy and dry seasons (Gilbert et al., 2015; Tagesson et al.,  
5 2016a; Räsänen et al., 2017). On the contrary, forest areas over Central Africa show the highest GPP  
6 estimates with values up to  $8 \text{ g m}^{-2} \text{ day}^{-1}$ . This is one of the wettest parts of the continent with three  
7 common peak rainfall periods: March-April-May (MAM), July-August-September (JAS) and October-  
8 November-December (OND). There is a marked north-south split in Europe, with very wet conditions  
9 in Scandinavia and very dry conditions in much of central and south-east Europe. A reduction of GPP  
10 gaps due to cloud cover up to 72% is obtained when the daily  $f_{\text{APAR}}$  time series are filtered and  
11 reconstructed, located mainly in central Africa ( $10^{\circ}\text{S}$ - $10^{\circ}\text{N}$ ) and high latitudes ( $>60^{\circ}\text{N}$ ).

12 [INSERT FIGURE 2]

#### 13 **4.2 Direct comparison with *in situ* EC tower GPP estimates**

14 Figure 3 shows the daily MSG GPP and the *in situ* EC GPP estimates from the FLUXNET EC towers (EC  
15 GPP). The MODIS and FLUXCOM GPP are also included for reference. The MSG GPP reproduces the  
16 seasonal variability in the EC GPP well, with low productivity values during winter and highest values  
17 during spring and summer. The MSG GPP time series show good performance to capture the GPP  
18 dynamics ( $r$  between 0.49 and 0.92) during the growing season, but less accurate in replicating GPP  
19 magnitude (rRMSE between 30% and 90%), which is mainly determined by  $\varepsilon_{\text{max}}$  (Fig. 2). At very high  
20 latitudes (e.g. North Europe), MSG GPP usually presents more gaps due to  $f_{\text{APAR}}$  missing values during  
21 winter. No MSG  $f_{\text{APAR}}$  values are calculated over areas covered by snow, by clouds during long  
22 periods, or with large uncertainties in the BRDF data (LSA SAF, 2016b).

23 [INSERT FIGURE 3]

24 The RS GPP products generally present a similar pattern (more detailed comparison is presented in  
25 section 5). For ENF, one of the most productive vegetation types considered in the present study  
26 (e.g. EC sites in Finland, Italy and Germany), a mean biased error (MBE) lower than 40% is observed  
27 in most of the towers (Table 2) with a high agreement between MSG GPP and EC GPP values ( $r>0.7$ ).  
28 As might be expected, over ENF sites, MSG shows very low GPP in winter and peak GPP in summer. In  
29 these cases, the AET and PET show similar values (Figure 4), confirming that such sites do not suffer  
30 water stress and main driving factors are radiation and temperature. A reduction of GPP gaps up to  
31 56% is obtained for these sites when the daily  $f_{\text{APAR}}$  values are filtered (e.g. De-Sfn). The differences  
32 are assessed by means of the root mean square error (RMSE). The highest ENF EC towers

1 disagreement is observed for FI-Let (RMSE=3.9 g m<sup>-2</sup> day<sup>-1</sup>), and IT-Lav (RMSE =3.4 g m<sup>-2</sup> day<sup>-1</sup>). A  
2 lower overall error and bias (RMSE=2.76 g m<sup>-2</sup> day<sup>-1</sup> and MBE=-1.34 g m<sup>-2</sup> day<sup>-1</sup>) are obtained when  
3 considering all ENF sites (Figure 5), observing a better agreement at EC GPP values lower than 7.0 g  
4 m<sup>-2</sup> day<sup>-1</sup> (distribution close to the 1:1 line).

5 For broadleaf flux towers, moderate ( $r=0.69$  for FR-Pue) to very good agreement ( $r=0.92$  for DE-Lnf)  
6 is observed between MSG GPP and EC GPP. The MSG GPP estimates agree with MODIS and  
7 FLUXCOM values, but the high EC GPP levels are not reached (e.g. DN-Lnf and Dk-Sor) giving an  
8 overall negative bias and RMSE= 3.62 g m<sup>-2</sup> day<sup>-1</sup> when all DBF towers are considered. For BE-Vie, DK-  
9 Sor, De-Lnf and DE-Hai discrepancies between the GLC2000 and the information provided by the  
10 tower (Table 1) are observed. These discrepancies are also present for the grassland (De-Gri, IT-MBo  
11 and SN-Dhr) and the savanna (ES-LMa, ZA-Kru) EC towers.

12 For grasslands towers IT-MBo and De-Gri, high correlations are observed (e.g.  $r$  up to 0.9 for IT-MBo).  
13 Although the main land cover type at both towers footprint is grassland, 72% of the land cover inside  
14 the 5 × 5 km area was determined as forest. The MSG GPP product is able to reproduce the seasonal  
15 behavior of this mixed forest (i.e. forest and grasslands) with large assimilation fluxes during the  
16 growing season (April-October) and to capture the GPP sharply decreased after the grass is mown in  
17 summer (i.e. DOY=180 for IT-MBo and De-Gri and DOY=210 for DE-Gri).

18 For the grassland (SN-Dhr) and savanna (ES-LMa) towers respectively in Senegal and Spain, the very  
19 high PET values when compared to AET (Figure 4) indicate a high water demand during all year. Thus,  
20 accounting for water stress effect by means of the ratio AET/PET is a key feature of MSG GPP product  
21 at these sites. In the case of SN-Dhr, a low agreement of MSG GPP with the EC GPP estimates (and  
22 also MODIS and FLUXCOM) during the growing season is observed. The vegetation phenology  
23 maximum is generally not reached during solar solstice for semi-arid ecosystems since its seasonal  
24 variability is rather controlled by water availability (Tagesson et al., 2016a). In this case, the GPP is  
25 essentially driven by  $f_{APAR}$  as also suggested when the seasonal patterns of GPP and  $f_{APAR}$  (Figure 4)  
26 are compared. For grasslands and savanna, a higher agreement (RMSE=2.11 g m<sup>-2</sup> day<sup>-1</sup>; MBE=-0.63 g  
27 m<sup>-2</sup> day<sup>-1</sup>) is observed between the MSG GPP and EC GPP estimates with a 60% of the EC GPP  
28 variance explained by the MSG GPP (Figure 5d).

29 [INSERT TABLE 2]

30 [INSERT FIGURE 4]

31 [INSERT FIGURE 5]

### 1 4.3 Consistency checking with synergistic global satellite carbon products

2 The MSG GPP provides similar or lower errors than MODIS and FLUXCOM at seven of the twelve  
3 forest towers when compared with *in situ* EC GPP (Table 1; CZ-BK1, FI-Sod, IT-Lav, De-Hai, IT-Col, Be-  
4 Vie and FR-Pue), as well as at ES-LMa and SN-Dhr sites (Table 3). In general, an underestimation is  
5 observed for the three RS products, being larger at the most productive DBF and ENF sites, such as  
6 DK-Sor, DE-Hai, DE-Lnf and FI-Let.

7 An overestimation is observed at two broadleaf forest towers (IT-Col and FR-Pue) and at DE-SfN  
8 during the growing season. At DE-SfN, the three RS products show higher values than EC GPP  
9 whereas FLUXCOM provides lower values at IT-Col and FR-Pue. At FR-Pue, the MODIS and FLUXCOM  
10 products show, respectively, the highest and lowest GPP estimates, whereas MSG GPP provides  
11 intermediate GPP values, more in agreement with the EC flux tower (i.e. MBE =  $0.7 \text{ g m}^{-2} \text{ day}^{-1}$ ,  
12 RMSE =  $1.8 \text{ g m}^{-2} \text{ day}^{-1}$  at 8-day temporal resolution). A higher constant MODIS  $f_{\text{APAR}}$  value ( $\sim 0.7$  at  
13 <https://modis.ornl.gov/fixedsite/>) than MSG  $f_{\text{APAR}}$  during all year along with the maximum value of  
14 radiation at the growing season could explain the higher GPP levels obtained for MODIS GPP. The  
15 highest discrepancy between the three RS products and EC GPP are observed for DK-Sor, DE-Hai, and  
16 FI-Let sites.

17 In general, a good agreement is observed between the MSG GPP and EC GPP estimates when the  
18 MSG GPP is re-sampled to 8-day and monthly temporal resolution (Figure 6a and 6b). The computed  
19 statistics are in agreement with those derived for the MODIS product. A MBE lower than  $1.5 \text{ g m}^{-2}$   
20  $\text{day}^{-1}$  is obtained for all the canopies. Although the higher RMSE is still observed for the DBF land  
21 cover, it is still lower than MODIS outcomes. At monthly temporal resolution, the MSG GPP errors  
22 decrease when considering all the EC towers except those corresponding to ENF and DBF (MBE <  $1.08$   
23  $1.0 \text{ g m}^{-2} \text{ day}^{-1}$ ), being lower than those observed for the FLUXCOM product.

24 [INSERT TABLE 3]

25 [INSERT FIGURE 6]

26 The differences between MSG with MODIS and FLUXCOM are spatially assessed by means of the  
27 annual root mean square difference (RMSD) and mean bias difference (MBD) (Figure 7). For Europe,  
28 the differences between the three RS products are very low. The differences are slightly lower when  
29 the MSG and MODIS are compared, particularly over South Europe and North and South Africa. The  
30 major GPP disagreement arises over moist biomes (e.g. tropical forests in central Africa) with RMSD  
31 values up to  $3.0 \text{ g m}^{-2} \text{ day}^{-1}$  and over dry biomes (e.g. semi-arid, savanna and transitional woodlands)

1 with MSG GPP estimates lower than FLUXCOM (e.g. MBD values up to  $-3.0 \text{ g C m}^{-2} \text{ day}^{-1}$ ).  
2 Particularly, MODIS and FLUXCOM provide larger differences for the humid savanna ecosystems of  
3 west and central Africa (MBD values up to  $2.0 \text{ g m}^{-2} \text{ day}^{-1}$ ).

4 [INSERT FIGURE 7]

5 The annual spatial patterns for MSG, MODIS, and FLUXCOM GPP (Figure 8) are compared. The three  
6 estimates agree reasonably well, although differences are significant in some areas. Specifically,  
7 there is a good agreement in Europe and North and South Africa, but MSG GPP is lower than  
8 FLUXCOM and MODIS over Central Africa. The largest differences occur in Equatorial areas covered  
9 by tropical forest where MODIS and FLUXCOM estimates are around  $3500 \text{ g m}^{-2} \text{ yr}^{-1}$ , while annual  
10 MSG GPP is below  $3000 \text{ g m}^{-2} \text{ yr}^{-1}$ .

11 [INSERT FIGURE 8]

## 12 5. Discussion

13 The retrieval of MSG GPP estimates from an optimized Monteith's model is presented. The MSG GPP  
14 product reproduces the EC GPP and its seasonal variability over most ecosystems. MBE values lower  
15 than 40% in most of the towers are found for the most efficient forest vegetation types. These MSG  
16 GPP values lie within the total uncertainty range for EC GPP proposed by Schaefer et al. (2012) as  
17 well as those obtained with coarse spatial resolution derived products (e.g. the Soil Moisture Active  
18 Passive global GPP product at 9 km (Kimball et al., 2016)). For the MODIS GPP product, average  
19 errors of 50% for non-forested ecosystems and larger underestimation (61%) for croplands were  
20 reported by Yang et al. (2007). The current MOD17A2 product is highly effective for MF (mixed  
21 forests) and DBF, moderately effective for ENF, and ineffective for EBF (Tang et al., 2015). Several  
22 factors have been discussed among possible causes for such differences that could also explain MSG  
23 GPP disagreements. These include diffusion radiation (Jenkins et al., 2007),  $f_{\text{APAR}}$  estimates (Zhao et  
24 al., 2011), the maximum light use efficiency (Yang et al., 2007), or differences in spatiotemporal  
25 coverage (Heinsch et al., 2006; Yang et al., 2007).

26 Particularly, the MSG GPP product shows a high ability to cope with water stress during the dry  
27 season at sites in Senegal and Spain (SN-Dhr and ES-LMa). Both sites are a typical low tree and shrub  
28 savanna environment with a low tree cover (Tagesson et al., 2015; Sánchez-Ruiz et al., 2017).  
29 However, larger discrepancies with EC GPP are found during the growing season, especially at SN-  
30 Dhr. Tagesson et al. (2017) explained the strong underestimation of the MODIS GPP product for the  
31 Sahel arguing that the  $\epsilon_{\text{max}}$  is set too low ( $\sim 0.85 \text{ g MJ}^{-1}$ ) in relation to *in situ* based estimates (1.58–

1 3.50 g MJ<sup>-1</sup>). Additionally, the EC GPP in SN-Dhr is high in relation to other semi-arid ecosystems;  
2 these high values have been explained, among others, by relatively dense ground vegetation and  
3 high soil nutrient availability (Tagesson et al., 2016a; Tagesson et al., 2016b). These parameters are  
4 not included in the satellite-based models possibly explaining these discrepancies. However, the low  
5 RMSE obtained in SN-Dhr and ES-LMa still indicate the strong applicability of the AET/PET ratio as a  
6 limiting factor in the Monteith model for drylands.

7 Furthermore, main uncertainties may be associated to scale mismatches between the EC footprint  
8 and the RS data. This could explain the highest disagreement observed for some of ENF (e.g. FI-Let,  
9 DE-SfN and IT-Lav) between the EC GPP and the GPP derived from the RS products. At DE-SfN, the  
10 canopy belongs to a natural peatland forest dominated by slow growing bog-pines and ground layer  
11 vegetation dominated by peat mosses (Hommeltenberg et al., 2014). As pine dominates the  
12 vegetation in the footprint area of the EC tower, the early rise of GPP (EC GPP and MSG GPP) in the  
13 year is likely due to the early start of photosynthesis of pine. During the course of the year, the  
14 overestimation of GPP in summer by the MSG GPP approach may also be a result of the pine  
15 dominated GPP which is lower compared to the classical peatbog vegetation. Although the  
16 overestimation is observed for the RS products, the early rise of EC GPP is only captured by the MSG  
17 GPP product. At IT-Lav, the forest is dominated by coniferous trees, but the EC site  
18 representativeness showed 32% cover by mixed forest and 8% by DBF, which explains the GPP lower  
19 values for MSG GPP and the temporal delay that the RS GPP products show at the beginning of the  
20 growing season. The FI-Let tower is a very homogeneous site compound by a mixture of scots pine  
21 and pubescent birch in the dominant canopy layer (Korkiakoski et al., 2017). In this site, the favorable  
22 water conditions (AET and PET ratio close to one) along with expected  $f_{APAR}$  and PAR values lead to  
23 think in other limiting factors that may affect the GPP predictions. (1) The SEVIRI/MSG observation  
24 geometry causes large uncertainties, mainly in wintertime, as a combination of multiple effects, such  
25 as low illumination angles, higher anisotropy, higher cloud occurrence, larger shadows or traces of  
26 snow cover. (2) GPP of forest ecosystems at high latitudes (>60°N) is greatly limited by low air  
27 temperature, a short growing season, and radiation availability (Anav et al., 2015).

28 The mismatch between the EC footprint and the MSG pixel size can also explain the diminution of  
29 GPP on DBF towers at the end of the summer (DE-Hai, DE-Lnf, DK-Sor). However, the MSG GPP  
30 discrepancies found for DBF at Denmark and Germany (e.g. DK-Sor, DE-Hai and DE-Lnf) could be  
31 reduced if the  $\epsilon_{max}$  would be better adjusted. At DK-Sor and DE-Hai, a crop  $\epsilon_{max}=1.2$  g MJ<sup>-1</sup> was set  
32 instead of a deciduous broadleaf forest  $\epsilon_{max}=1.8$  g MJ<sup>-1</sup>, substantially lowering MSG GPP. A reduction  
33 of rMBE respectively to 31% and 6% could be achieved if  $\epsilon_{max}$  would be adjusted accordingly. Quaife

1 et al. (2008) estimated that the error in GPP introduced from satellite derived land cover is up to  
2 16%. An overall accuracy of 68.6% was reported for GLC2000 at a global scale (Mayaux et al., 2006).  
3 Thus, the wrong assignment of GLC2000 classes has a negative impact on MSG GPP values where a  
4 more accurate land cover map would thereby improve the performance of the MSG GPP product.

5 Another important factor that limits photosynthesis is cloud cover. Although the reduction of carbon  
6 uptake by photosynthesis due to cloud cover is primarily assumed by the diminution of the radiation  
7 input, the GPP estimates could be limited by the reliability of biophysical parameters such as  $f_{APAR}$   
8 and leaf area index due to the lack of an operational and efficient cloud filtering. The filter and  
9 reconstruction of the MSG  $f_{APAR}$  time series allowed reducing the overall error of the GPP estimates.  
10 When the three RS products are intercompared, the observations used for the comparison may differ  
11 due to the availability and nominal temporal sampling interval, which could be hampered by missing  
12 data mainly due to cloud occurrence. In case of MSG GPP, the daily basis will allow performing gap  
13 filling and filtering techniques for an accurate depiction of vegetation dynamics and correct the  
14 diminution of GPP due to spectral cloud contamination, as it takes place on tropical forests.

15 At regional level, the MSG GPP estimates are similar to MODIS and FLUXCOM ones over the  
16 temperate zones whereas the largest discrepancies are observed over the tropical zone. In the  
17 tropics, large differences are also detected between MODIS and FLUXCOM. A poor relatively  
18 FLUXCOM GPP prediction was expected in the tropics due to an undersampled training data  
19 (Tramontana et al., 2016). Differences could also be attributed to GPP low quality due to  
20 contamination from cloudiness (i.e. affecting MSG and MODIS  $f_{APAR}$  products) and poor constraints on  
21 meteorological reanalysis datasets affecting MODIS GPP product (Zhao and Running, 2006).  
22 Moreover, the underestimation of MSG GPP values for the tropical region may be explained by, i)  
23 systematic low MSG  $f_{APAR}$  values reported over needleleaf and broadleaf forests (Martinez et al.,  
24 2013) and ii) uncertainties introduced by an overestimation of PET derived from the JS approach over  
25 broadleaf forest (Vörösmarty et al., 1998). This pattern is consistent with the finding by Zhao et al.  
26 (2006), which showed that the tropical region has the largest uncertainties in MODIS GPP.

27 The selection of only one year was justified by a trade-off between the availability of necessary input  
28 data for the other years from LSA-SAF and the major representativeness of EC GPP data for validation  
29 purposes. To evaluate the reliability and performance of the method for daily MSG GPP retrievals it  
30 was required to capture and monitor the GPP magnitude and seasonal variability for at least one  
31 year. However, a longer GPP time-series consisting of inter-annual variability would improve the  
32 model evaluation and this is possible as the data availability from LSA-SAF increases. Additionally, as  
33 new MSG products appear in the LSA SAF system, these can be incorporated in the  $C_{ws}$

1 parameterization to improve the model accuracy, such as the daily reference evapotranspiration  
2 (DMETREF, LSA-303).

### 3 **6. Summary and conclusions**

4 This study aimed to provide a method for daily GPP estimates over Europe and Africa based on an  
5 ensemble of SEVIRI/MSG available products. The proposed framework takes advantage of the LSA  
6 SAF system facilities, and uses operational SEVIRI/MSG products to measure the absorbed  
7 photosynthetic active radiation (APAR) by vegetation (i.e. the product by PAR and  $f_{APAR}$ ) and the  
8 environmental variables that affect the use of this absorbed flux in primary production (Trigo et al.,  
9 2011). This newly derived product has the potential for analyzing spatial patterns and temporal  
10 dynamics of GPP at the MSG spatial resolutions on a daily basis. The real challenge was to capture  
11 GPP dynamics and magnitude during the growing season. We would like to highlight the MSG GPP  
12 performance in relation to three aspects:

13 1) The ability to capture the intra-annual variability of carbon cycle. The new MSG GPP product has a  
14 daily temporal resolution, which is a major advantage in relation to previous satellite based GPP  
15 products in the study of intra-annual dynamics of GPP.

16 2) The capability to identify possible reduction of productivity due to water shortage which is very  
17 important in dry-lands. The MSG GPP estimates introduce the advantage of considering the  $C_{ws}$  water  
18 stress factor by means of a global AET product generated also with MSG data as well as a  
19 parameterized potential ET by means of air temperature.

20 3) The potential to provide a new GPP product with at least equally high confidence as compared to  
21 other satellite derived GPP products. An evaluation against independent *in situ* data indicated that  
22 the uncertainties of the daily MSG GPP estimates are similar to those shown by other satellite  
23 products, such as MODIS and FLUXCOM.

24 This study broadens the applicability of SEVIRI/MSG products for deriving reliable carbon uptake  
25 estimates over Europe and Africa. The coarser spatial resolution of SEVIRI is compensated by the  
26 availability of combining different MSG products at daily temporal coverage that can contribute to  
27 increased knowledge regarding changes in GPP (e.g. daily, seasonally or yearly) as well as higher  
28 precision in GPP accumulated values.

### 29 **ACKNOWLEDGEMENTS**

1 This research was supported by the LSA SAF (EUMETSAT) and ESCENARIOS project from the Spanish  
2 Ministry of Economy and Competitiveness (CGL2016-75239-R). This work used eddy covariance data  
3 acquired and shared by the FLUXNET community. The FLUXNET eddy covariance data processing and  
4 harmonization was carried out by the European Fluxes Database Cluster, AmeriFlux Management  
5 Project, and Fluxdata project of FLUXNET, with the support of CDIAC and ICOS Ecosystem Thematic  
6 Center, and the OzFlux, ChinaFlux and AsiaFlux offices. The ERA-Interim reanalysis data were  
7 provided by ECMWF and processed by LSCE. We also thank M. Jung for providing FLUXCOM GPP. The  
8 funding of SNSB (Dnr 95/16) for T.Tagesson and the Helmholtz Association and the Federal Ministry  
9 of Education and Research (BMBF) in the framework of TERENO (Terrestrial Environmental  
10 Observatories) and ICOS (Integrated Carbon Observation System) are also acknowledged.

## 11 REFERENCES

- 12 Anav, A., et al., 2015. Spatiotemporal patterns of terrestrial gross primary production: A review. *Rev.*  
13 *Geophys.*, 53, 785–818, doi:10.1002/2015RG000483.
- 14
- 15 Bartholomé, E., Belward, A.S. 2005. GLC2000: a new approach to global land cover mapping from  
16 Earth observation data. *International Journal of Remote Sensing* 26, (9), 1959–1977.
- 17
- 18 EEA, 2012. Climate change, impacts and vulnerability in Europe 2012. An indicator-based report, EEA  
19 Report No 12/2012, European Environment Agency, Copenhagen, Denmark.
- 20
- 21 Fisher, J.B., Whittaker, R.J., Malhi, Y. 2011. ET come home: potential evapotranspiration in  
22 geographical ecology. *Global Ecology and Biogeography*, 20, 1–18.
- 23
- 24 Garbulsky, M.F., et al., 2010. Patterns and controls of the variability of radiation use efficiency and  
25 primary productivity across terrestrial ecosystems. *Glob. Ecol. Biogeogr.*, 19, 253–267.
- 26
- 27 García-Haro, F.J., Camacho, F., Martínez, B., Meliá, J. 2015. Validation Report Vegetation Parameters  
28 (VEGA), SAF/LAND/UV/VR\_VEGA/2.0. Available on-line at <<http://landsaf.meteo.pt>>.
- 29
- 30 Geiger, B., Meurey, C., Lajas, D., Franchistéguy, L., Carrer, D., Roujean, J-L. 2008. Near real time  
31 provision of downwelling shortwave radiation estimates derived from satellite observations.  
32 *Meteorological Applications*, 2008, 15, 411-420.
- 33
- 34 Gilabert, M.A., et al., 2015. Daily GPP estimates in Mediterranean ecosystems by combining remote  
35 sensing and meteorological data. *ISPRS Journal of Photogrammetry and Remote Sensing*, 102, 184–  
36 197.
- 37
- 38 Heinsch, F. A., et al., 2006. Evaluation of remote sensing based terrestrial productivity from MODIS  
39 using regional tower eddy flux network observations, *IEEE Trans. Geosci. Remote Sens.*, 44 (7), 1908–  
40 1925.
- 41
- 42 Hommeltenberg, J., Schmid, H.P., Drösler, M., Werle, P. 2014. Can a bog drained for forestry be a  
43 stronger carbon sink than a natural bog forest?. *Biogeosciences*, 11, 3477–3493.
- 44
- 45 Iqbal, M., 1983. *An Introduction to Solar Radiation*. Academic Press, Toronto, 390pp.

1  
2 Idso, S.B., Jackson, R.D., Pinter, P.J., Reginato, R.J., Hatfield, J.L. 1981. Normalizing the stress-degree-  
3 day parameter for environmental variability. *Agricultural and Forest Meteorology* 24, 45–55.  
4  
5 IPCC. 2014. *Climate Change 2014: Impacts, Adaptation, and Vulnerability*, Cambridge University  
6 Press, Cambridge, United Kingdom and New York, NY, USA.  
7  
8 Jensen, M.E., Haise, H.R. 1963. Estimating evapotranspiration from solar radiation. *J. Irriga. Drain.*  
9 *Div.* 89, 15–41.  
10  
11 Jung, M., et al., 2017. Compensatory water effects link yearly global land CO<sub>2</sub> sink changes to  
12 temperature. *Nature*, 541, doi:10.1038/nature20780.  
13  
14 Kimball, J. S., Jones, L.A., Glassy, J., Stavros, E.N., Madani, N., Reichle, R.H., Jackson, T., Colliander, A.  
15 2016. Soil Moisture Active Passive (SMAP) Mission Assessment Report for the Version 2 Validated  
16 Release L4\_C Data Product. GMAO Office Note No. 13 (Version 1.0), 37 pp, NASA Goddard Space  
17 Flight Center, Greenbelt, MD, USA.  
18  
19 Korkiakoski, M., et al., 2017. Methane exchange at the peatland forest floor – automatic chamber  
20 system exposes the dynamics of small fluxes. *Biogeosciences*, 14, 1947-1967, doi:10.5194/bg-14-  
21 1947-2017.  
22  
23 Kumar, J., Hoffman, F. M., Hargrove, W.W., Collier, N. 2016. Understanding the representativeness of  
24 FLUXNET for upscaling carbon flux from eddy covariance measurements. *Earth System Science Data*  
25 *Discussion*, doi:10.5194/essd-2016-36.  
26  
27 Lasslop, G., et al., 2010. Separation of net ecosystem exchange into assimilation and respiration using  
28 a light response curve approach: Critical issues and global evaluation, *Global Change Biol.*, 16, 187–  
29 208, doi:10.1111/j.1365-2486.2009.02041.x.  
30  
31 LSA SAF. 2010. Algorithm Theoretical Basis Document (ATBD) for MSG Evapotranspiration (MET) and  
32 daily MET (DMET) product. SAF/LAND/IM/ATBD\_MET/1.2. Available on-line at  
33 <<http://landsaf.meteo.pt>>.  
34  
35 LSA SAF. 2012. Algorithm Theoretical Basis Document (ATBD) for Down-welling Surface Shortwave  
36 Flux (DSSF). SAF/LAND/MF/ATBD\_DSSF/1.0. Available on-line at <<http://landsaf.meteo.pt>>.  
37  
38 LSA SAF. 2016a. Algorithm Theoretical Basis Document (ATBD) for Reference Evapotranspiration  
39 (DMETREF). SAF/LAND/IPMA/ATBD\_METREF/1.0. Available on-line at <<http://landsaf.meteo.pt>>.  
40  
41 LSA SAF. 2016b. Algorithm Theoretical Basis Document for Vegetation parameters (VEGA).  
42 PRODUCTS: LSA-421 (MDFVC), LSA-422 (MTFVC), LSA-423 (MDLAI), LSA-424 (MTLAI), LSA-425  
43 (MDFAPAR), LSA-426 (MTFAPAR), LSA-450 (MTFVCR), LSA-451 (MTLAI-R), LSA-452 (MTFAPAR-R).  
44 SAF/LAND/UV/VR\_VEGA/2.0. Available on-line at <<http://landsaf.meteo.pt>>.  
45  
46 Martínez, B., Camacho, F., Verger, A., García-Haro, F.J., Gilabert, M.A. 2013. Intercomparison and  
47 quality assessment of MERIS, MODIS and SEVIRI FAPAR products over the Iberian Peninsula. *Int. J.*  
48 *Appl. Earth Obs. Geoinf.* 21, 463–476.  
49  
50 Maselli, F., Papale, D., Puletti, N., Chirici, G., Corona, P., 2009. Combining remote sensing and  
51 ancillary data to monitor the gross productivity of water-limited forest ecosystems. *Remote Sens.*  
*Environ.* 113, 657–667.

1  
2 Maselli, F., Argenti, G., Chiesi, M., Angeli, L., Papale, D., 2013. Simulation of grassland productivity by  
3 the combination of ground and satellite data. *Agric. Ecosyst. Environ.* 165, 163–172.  
4  
5 Mayaux, P., et al., 2006. Validation of the Global Land Cover 2000 Map. *IEEE Trans. Geosci. Remote*  
6 *Sens.*, 44 (7), 1728–1739.  
7  
8 Monteith, J.L., 1972. Solar radiation and productivity in tropical ecosystems. *J. Appl. Ecol.* 9, 747–766.  
9  
10 Moreno, A., Gilabert, M.A., Camacho, F., Martínez, B. 2013. Validation of daily global solar irradiation  
11 images from MSG over Spain. *Renew. Energy* 60, 332–342.  
12  
13 Moreno, A., García-Haro, F.J., Martínez, B., Gilabert, M.A., 2014. Noise reduction and gap filling of  
14 fAPAR series using an adapted local regression filter. *Rem. Sens.* 6, 8238–8260.  
15 <http://dx.doi.org/10.3390/rs6098238>.  
16  
17 Nemani, R. R., Keeling, C. D., Hashimoto, H., Jolly, W. M., Piper, S. C., Tucker, C. J., et al., 2003.  
18 Climate-driven increases in global terrestrial net primary production from 1982 to 1999. *Science*, 300,  
19 1560– 1563.  
20  
21 Papale, D., Valentini, R. 2003. A new assessment of European forests carbon exchanges by eddy  
22 fluxes and artificial neural network spatialization, *Glob. Change Biol.*, 9, 525–535, doi:10.1046/j.1365-  
23 2486.2003.00609.x.  
24  
25 Pastorello, G., et al., 2014. Observational Data Patterns for Time Series Data Quality Assessment, in:  
26 e-Science (e-Science), 2014 IEEE 10th International Conference on, vol. 1, pp. 271–278,  
27 doi:10.1109/eScience.2014.45.  
28  
29 Räsänen, M., et al., 2017. Carbon balance of a grazed savanna grassland ecosystem in South Africa.  
30 *Biogeosciences*, 14, 1039–1054, doi:10.5194/bg-14-1039-2017.  
31  
32 Roujean, J.L., Bréon, F.M. 1995. Estimating PAR absorbed by vegetation from bidirectional  
33 reflectance measurements. *Remote Sens. Environ.*, 51, 373–384.  
34  
35 Running, S. W., Nemani, R.R., Heinsch, F.A., Zhao, M., Reeves, M., Hashimoto, H. 2004. A continuous  
36 satellite-derived measure of global terrestrial primary productivity: Future science and applications,  
37 *BioScience*, 56(6), 547–560.  
38  
39 Running, S. W., Zhao, M. 2015. Daily GPP and Annual NPP (MOD17A2/A3) Products NASA Earth  
40 Observing System MODIS Land Algorithm. User's Guide. Version 3.0 For Collection 6.  
41  
42 Sánchez-Ruiz, S., Moreno, A., Piles, M., Maselli, F., Carrara, A., Running, S., Gilabert, M.A. 2017.  
43 Quantifying water stress effect on daily light use efficiency in Mediterranean ecosystems using  
44 satellite data, *International Journal of Digital Earth*, 10 (6), 623-638.  
45  
46 Schaefer, K., et al., 2012. A model-data comparison of gross primary productivity: Results from the  
47 North American Carbon Program site synthesis. *Journal of Geophysical Research*, 117, G03010,  
48 doi:10.1029/2012JG001960.  
49  
50 Sepulcre, G., Vogt, J., Arboleda, A, Antofie, T. 2014. Assessment of the EUMETSAT LSA-SAF  
51 evapotranspiration product for drought monitoring in Europe. *Int. J. Applied EO Geoinf*, 30, 190-202.  
52

1 Sjöström, M., et al., 2013. Evaluation of MODIS gross primary productivity for Africa using eddy  
2 covariance data, *Remote Sens. Environ.*, 131, 275–286.  
3  
4 Tagesson, T., Fensholt, R., Cropley, F., Guiro, I., Horion, S., Ehammer, A., Ardö, J. 2015. Dynamics in  
5 carbon exchange fluxes for a grazed semi-arid savanna ecosystem in West Africa, *Agr. Ecosyst.*  
6 *Environ.*, 205, 15–24, doi:10.1016/j.agee.2015.02.017.  
7  
8 Tagesson, T. et al., 2016a. Spatiotemporal variability in carbon exchange fluxes across the Sahel  
9 *Agric. For. Meteorol.*, 226–227: 108-118.  
10  
11 Tagesson, T. et al., 2016b. Very high carbon exchange fluxes for a grazed semi-arid savanna  
12 ecosystem in West Africa. *Danish Journal of Geography*, 116: 93-109.  
13  
14 Tagesson, T. et al., 2017. Modelling spatial and temporal dynamics of gross primary production in the  
15 Sahel from earth-observation-based photosynthetic capacity and quantum efficiency.  
16 *Biogeosciences*, 14, 5, 1333-1348.  
17  
18 Tang, X., Li, H., Huang, N., Li, X., Xu, X., Ding, D., Xie, J. 2015. A comprehensive assessment of MODIS-  
19 derived GPP for forest ecosystems using the site-level FLUXNET database. *Environ Earth Sci* (2015)  
20 74:5907–5918. DOI 10.1007/s12665-015-4615-0.  
21  
22 Tian, H., Chen, G., Liu, M., et al. 2010. Model estimates of net primary productivity,  
23 evapotranspiration, and water use efficiency in the terrestrial ecosystems of the Southern United  
24 States during 1895–2007. *Forest Ecology and Management*, 259, 7, 1311–1327.  
25  
26 Tramontana, G., et al. 2016. Predicting carbon dioxide and energy fluxes across global FLUXNET sites  
27 with regression. *Biogeosciences*, 13, 4291–4313, doi:10.5194/bg-13-4291-2016.  
28  
29 Trigo, I. F., et al., 2011. The Satellite Application Facility on Land Surface Analysis. *Int. J. Remote*  
30 *Sens.*, 32, 2725-2744, doi: 10.1080/01431161003743199.  
31  
32 Valentini, R., et al., 2014. A full greenhouse gases budget of Africa: synthesis, uncertainties, and  
33 vulnerabilities, *Biogeosciences*, 11, 381–407, doi:10.5194/bg-11-381-2014, 2014.  
34  
35 Van Wijk, M.T., Bouten, W. 1999. Water and carbon fluxes above European coniferous forests  
36 modeled with artificial neural networks. *Ecol. Mod.*, 120, 181–197.  
37  
38 Vörösmarty, C.J., Federer, C.A., Schloss, A.L. 1998. Potential evaporation functions compared on US  
39 watersheds: Possible implications for global-scale water balance and terrestrial ecosystem modelling.  
40 *Journal of Hydrology*, 207, 147–169.  
41  
42 Waring, H.R, Running, S.W., 2007. *Forest ecosystems analysis at Multiple Scales*, 3rd ed. Academic  
43 Press, San Diego.  
44  
45 Zarco-Tejada, P., Pushnik, J., Dobrowski, S., and Ustin, S. 2003. Steadystate chlorophyll a fluorescence  
46 detection from canopy derivative reflectance and double-peak red-edge effects, *Remote Sens.*  
47 *Environ.*, 84, 283–294, doi:10.1016/S0034-4257(02)00113-X.  
48  
49 Zhao, M., S. W. Running, Nemani, R.R. 2006. Sensitivity of Moderate Resolution Imaging  
50 Spectroradiometer (MODIS) terrestrial primary production to the accuracy of meteorological  
51 reanalyses, *J. Geophys. Res.*, 111, G01002, doi:10.1029/2004JG000004.  
52

1 Zhao, M., Running, S.W., 2010. Drought-induced reduction in global terrestrial net primary  
2 production from 2000 through 2009. *Science*, 329, 940–943.  
3

4 Zhao, M., Running, S.W., Heinsch, F.A., Nemani, R.R. 2011. MODIS derived terrestrial primary  
5 production. In: *Land Remote Sensing and Global Environmental Change*. Springer, New York, pp.  
6 635–660, [dx.doi.org/10.1007/978-1-4419-6749-7\\_28](http://dx.doi.org/10.1007/978-1-4419-6749-7_28).  
7

8 Yang, F., et al., 2007. Developing a continental-scale measure of gross primary production by  
9 combining MODIS and AmeriFlux data through support vector machine approach. *Remote Sens.*  
10 *Environ.*, 110, 109–122.  
11

12 Yebra, M., Van Dijk, A.I.J.M., Leuning, R., Guerschman, J.P. 2015. Global vegetation gross primary  
13 production estimation using satellite-derived light-use efficiency and canopy conductance. *Remote*  
14 *Sens. Environ.* 163, 206–216. <http://dx.doi.org/10.1016/j.rse.2015.03.016>.

## TABLES

**Table 1.** Description of EC sites located in Europe and Africa along with the main land cover percentage over a 5 km × 5 km GLC2000 window. The GLC2000 land cover of each site belongs to: CRO (croplands), DBF (deciduous broadleaf forest), EBF (evergreen broadleaf forest), ENF (evergreen needleleaf forest), MXF (mixed forest), SHR (shrublands), GRS (grasslands), or CRO (crops). PFT refers to the most representative plant functional type of the EC tower. SAV refer to savanna PFT.

Label	Name	Country	Latitude (°)	Longitude (°)	Altitude (m)	PFT	GLC2000	Main cover percentage (%)
CZ-BK1	Bily Kriz	Czech Republic	49,50	18,54	875	ENF	ENF	100
DE-SfN	Schechenfilz ord	Germany	47,81	11,33	590	ENF	ENF	80
FI-Let	Lettosuo	Finland	60,64	23,96	119	ENF	ENF	88
FI-Hyy	Hyytiala	Finland	61,85	24,29	181	ENF	ENF	80
FI-Sod	Sodankyla	Finland	67,36	26,64	180	ENF	ENF	92
IT-Lav	Lavarone	Italy	45,96	11,28	1353	ENF	ENF	44
DE-Hai	Hainich	Germany	51,08	10,45	430	DBF	CRO	72
DE-Lnf	Leinefelde	Germany	51,33	10,37	451	DBF	ENF	80
IT-Col	Collelongo	Italy	41,85	13,59	1560	DBF	DBF	96
DK-Sor	Soroe	Denmark	55,49	11,65	40	DBF	CRO	96
BE-Vie	Vielsalm	Belgium	50,31	5,99	493	DBF+ENF	ENF	92
FR-Pue	Puechabon	France	43,74	3,59	270	EBF	EBF	92
DE-Gri	Grillenburg	Germany	50,95	13,51	385	GRS	ENF	92
IT-MBo	Monte Bondone	Italy	46,01	11,05	1550	GRS	DBF	72
SN-Dhr	Dahra	Senegal	15,40	-15,43	40	GRS	CRO	100
Es-LMa	Las Majadas	Spain	39,94	-5,77	258	SAV	MXF	44
ZA-Kru	Skukuza	South Africa	-15,44	23,25	359	SAV	SHR	64
DE-Geb	Gebesee	Germany	51,10	10,91	161	CRO	CRO	100

**Table 2.** Statistics of the MSG GPP direct comparison between MSG GPP and GPP EC. The mean bias error (MBE), mean absolute error (MAE) and root mean square error (RMSE) are given in  $\text{g m}^{-2} \text{day}^{-1}$ , and their relative values (rMBE, rMAE and rRMSE) in %. The correlation coefficient (r) is also shown.

<b>SITE FLUXNET ID</b>	<b>MBE (rMBE)</b>	<b>MAE (rMAE)</b>	<b>RMSE (rRMSE)</b>	<b>r</b>
CZ-BK1	-1.3 (-29)	1.7 (36)	2.3 (50)	0.91
DE-SfN	-0.1 (-2)	1.1 (33)	1.4 (42)	0.85
FI-Let	-3.2 (-38)	3.3 (39)	3.9 (47)	0.71
FI-Hyy	-2.3 (-32)	2.5 (35)	3.1 (42)	0.72
FI-Sod	0.2 (4)	1.0 (17)	1.3 (25)	0.74
IT-Lav	-2.4 (-39)	2.5 (39)	3.4 (54)	0.88
DE-Hai	-1.6 (-35)	2.3 (52)	3.3 (75)	0.87
DE-Lnf	-2.2 (-45)	3.2 (65)	4.6 (94)	0.77
IT-Col	1.5 (36)	1.9 (46)	2.4 (57)	0.92
DK-Sor	-2.9 (-51)	3.2 (56)	4.7 (83)	0.88
BE-Vie	-2.1 (-35)	2.3 (38)	3.0 (50)	0.81
FR-Pue	0.7 (23)	1.4 (43)	1.9 (60)	0.69
DE-Gri	-0.6 (-13)	1.7 (40)	2.4 (56)	0.84
IT-MBo	-0.6 (-13)	1.6 (38)	2.3 (56)	0.90
SN-Dhr	-1.0 (-41)	1.3 (51)	2.3 (92)	0.89
ES-LMa	-0.1 (-4)	1.0 (49)	1.2 (58)	0.49
ZA-Kru	-1.1 (-28)	1.5 (37)	2.1 (52)	0.78
DE-Geb	-0.1 (-3)	1.3 (55)	1.8 (80)	0.73

Note: Correlations were statistically significant at 95% confidence level.

**Table 3.** Statistics resulting from the comparison of the three RS GPP products with the *in situ* EC GPP estimates. The MBE, MAE and RMSE are in  $\text{g m}^{-2} \text{day}^{-1}$ . The daily MSG GPP was resampled to the temporal resolution of MODIS (8 days) and FLUXCOM (1 month). The correlation coefficients (*r*) are presented.

		MBE	RMSE	r		MBE	RMSE	r
CZ-BK1	MSG <sub>8days</sub>	-1.5	2.2	0.97	MSG <sub>monthly</sub>	-1.3	1.9	0.99
	MODIS	-1.5	2.0	0.95	FLUXCOM	-1.8	2.3	0.89
DE-SfN	MSG <sub>8days</sub>	-0.1	1.0	0.91	MSG <sub>monthly</sub>	-0.2	1.0	0.88
	MODIS	-0.01	1.8	0.85	FLUXCOM	0.3	2.2	0.83
FI-Let	MSG <sub>8days</sub>	-3.1	3.6	0.81	MSG <sub>monthly</sub>	-2.6	3.1	0.85
	MODIS	-2.7	3.1	0.88	FLUXCOM	-2.9	3.2	0.92
FI-Hyy	MSG <sub>8days</sub>	-2.3	2.8	0.74	MSG <sub>monthly</sub>	-1.8	2.4	0.78
	MODIS	-1.9	2.3	0.87	FLUXCOM	-1.9	2.2	0.88
FI-Sod	MSG <sub>8days</sub>	-0.12	0.7	0.88	MSG <sub>monthly</sub>	0.1	0.3	0.98
	MODIS	-0.4	0.9	0.85	FLUXCOM	-2.0	2.1	0.88
IT-Lav	MSG <sub>8days</sub>	-2.3	3.2	0.90	MSG <sub>monthly</sub>	-2.8	3.4	0.92
	MODIS	-2.7	3.5	0.87	FLUXCOM	-4.2	4.4	0.89
DE-Hai	MSG <sub>8days</sub>	-1.6	3.2	0.91	MSG <sub>monthly</sub>	-1.4	2.9	0.91
	MODIS	-1.5	3.0	0.91	FLUXCOM	-1.1	2.9	0.78
DE-Lnf	MSG <sub>8days</sub>	-2.2	4.6	0.81	MSG <sub>monthly</sub>	-1.9	4.2	0.76
	MODIS	-2.3	4.2	0.88	FLUXCOM	-1.6	3.3	0.83
IT-Col	MSG <sub>8days</sub>	1.4	2.0	0.95	MSG <sub>monthly</sub>	1.7	2.1	0.95
	MODIS	-0.4	2.5	0.92	FLUXCOM	-1.4	3.1	0.83
DK-Sor	MSG <sub>8days</sub>	-2.8	4.6	0.90	MSG <sub>monthly</sub>	-2.7	4.3	0.91
	MODIS	-2.9	4.4	0.93	FLUXCOM	-2.8	4.2	0.92
BE-Vie	MSG <sub>8days</sub>	-2.1	2.7	0.88	MSG <sub>monthly</sub>	-1.9	2.6	0.87
	MODIS	-2.1	2.6	0.92	FLUXCOM	-1.2	2.0	0.88
FR-Pue	MSG <sub>8days</sub>	0.7	1.8	0.64	MSG <sub>monthly</sub>	0.7	1.5	0.78
	MODIS	2.0	3.2	0.67	FLUXCOM	-0.7	1.1	0.82
DE-Gri	MSG <sub>8days</sub>	-0.7	2.3	0.88	MSG <sub>monthly</sub>	-0.5	1.7	0.94
	GPP MODIS	-1.4	2.5	0.90	FLUXCOM	-1.8	2.4	0.92
IT-MBo	MSG <sub>8days</sub>	-0.4	1.9	0.93	MSG <sub>monthly</sub>	-0.6	2.1	0.96
	MODIS	-0.6	1.2	0.96	FLUXCOM	-1.0	2.0	0.91
SN-Dhr	MSG <sub>8days</sub>	-1.0	2.2	0.90	MSG <sub>monthly</sub>	-1.1	2.1	0.94
	MODIS	-1.3	2.6	0.90	FLUXCOM	-1.2	1.9	0.93
ES-LMa	MSG <sub>8days</sub>	-0.2	1.0	0.60	MSG <sub>monthly</sub>	0.02	0.8	0.63
	MODIS	-0.6	1.6	0.90	FLUXCOM	-0.6	1.1	0.57
ZA-Kru	MSG <sub>8days</sub>	-1.1	1.7	0.90	MSG <sub>monthly</sub>	-1.1	1.5	0.96
	MODIS	-0.7	1.6	0.80	FLUXCOM	-0.8	1.2	0.94
DE-Geb	MSG <sub>8days</sub>	-0.2	1.6	0.80	MSG <sub>monthly</sub>	0.1	1.3	0.80
	MODIS	-0.2	1.4	0.84	FLUXCOM	0.7	1.9	0.81

Note: Correlations were statistically significant at 95% confidence level.

## FIGURES

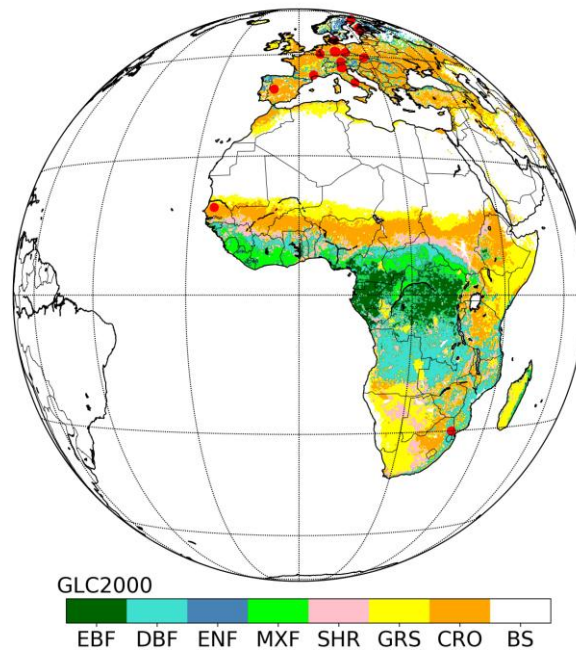


**Figure 1.** The Global Land Cover 2000 (GLC2000) is shown. The GLC2000 has been geo-located and resampled to a standard SEVIRI grid. The selected EC sites are also included (red circles). A generalized thematic legend of 6 major land covers has been proposed in order to reduce the number of classes while preserving the essence of the geographical patterns of the study area.

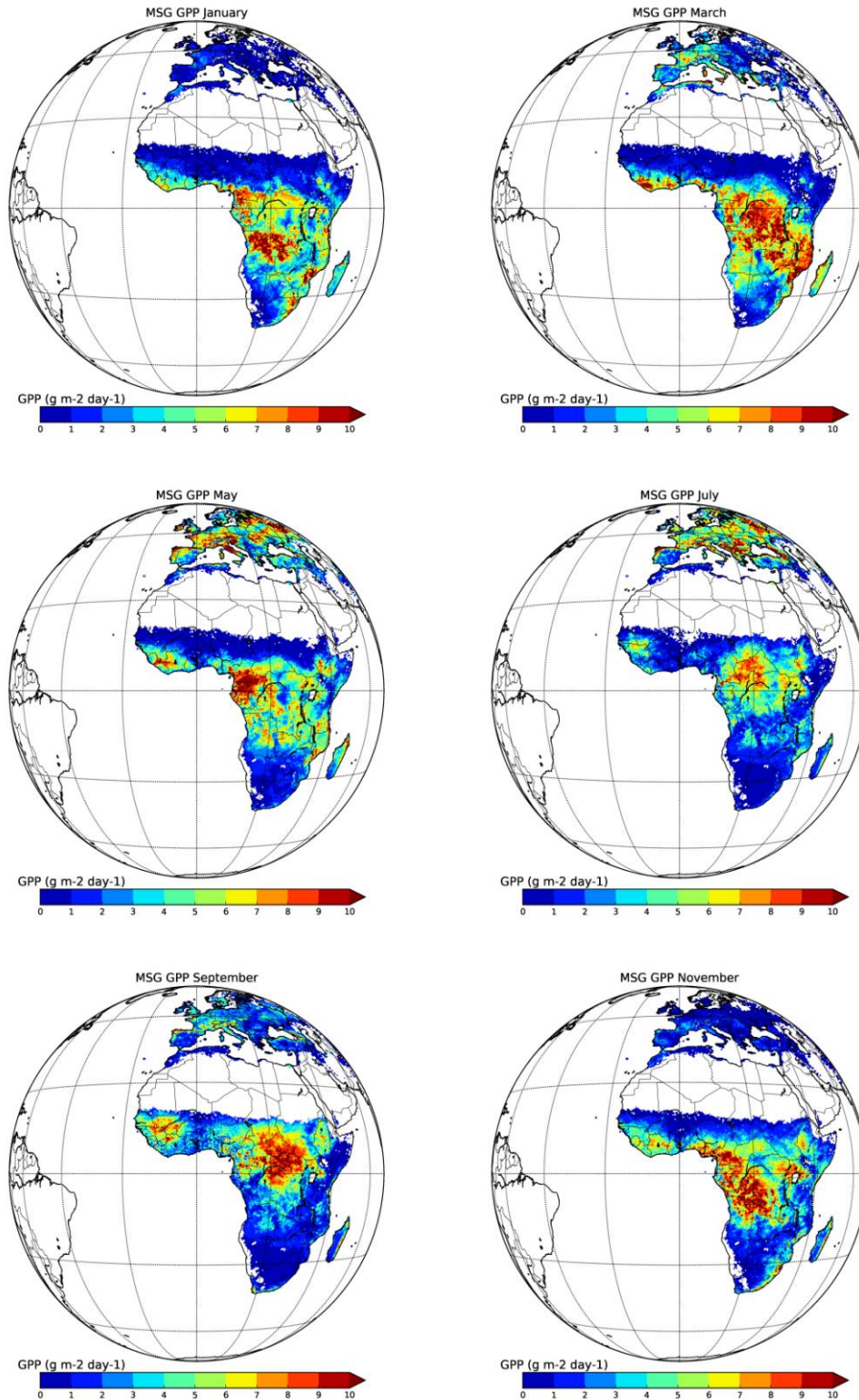


**Figure 2.** Daily MSG GPP ( $\text{g m}^{-2} \text{ day}^{-1}$ ) images for a particular day every two months in 2012. The day chosen was as close to the middle of the month as possible.

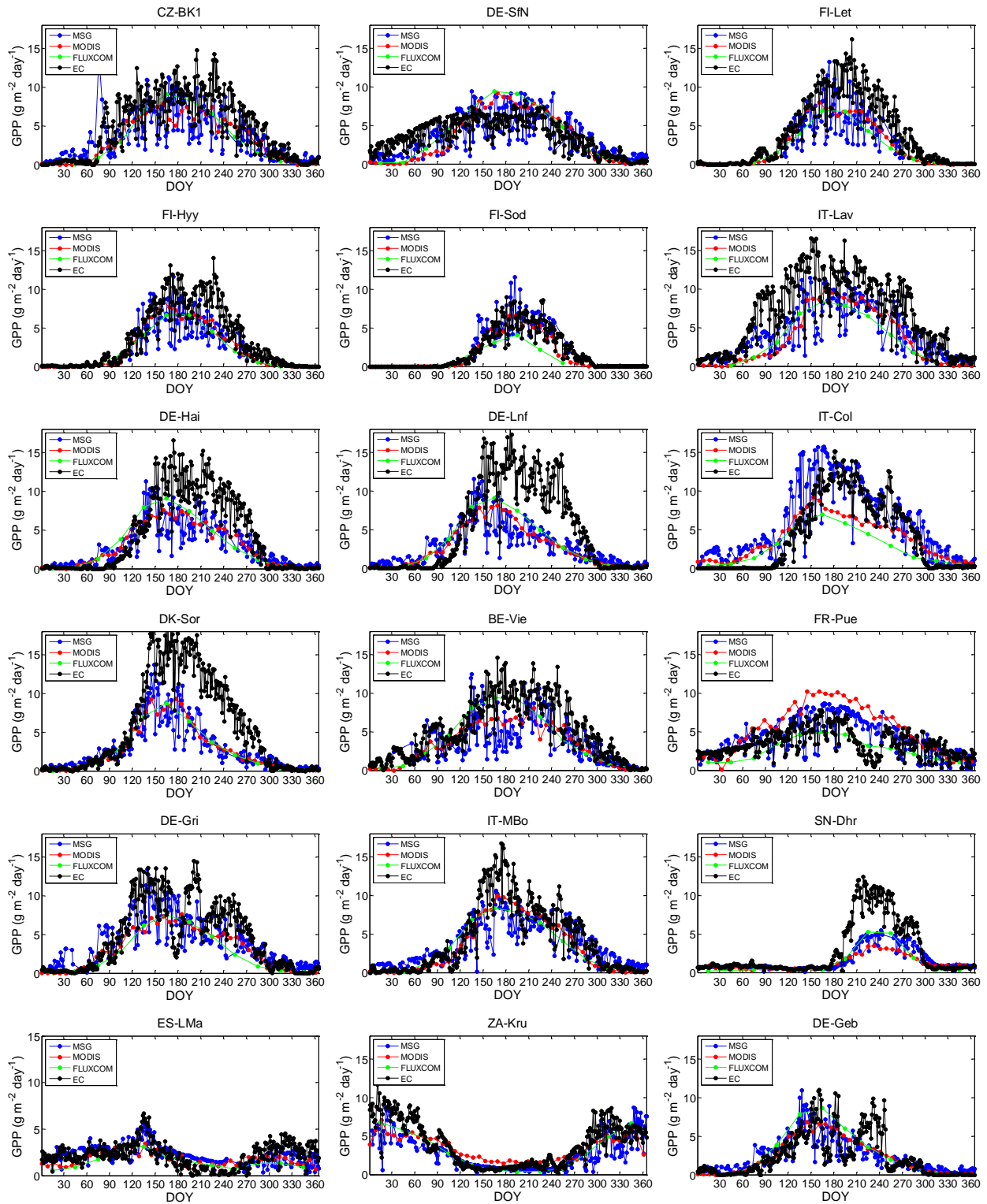


**Figure 3.** Temporal profiles of daily MSG GPP, 8-day MODIS GPP and monthly FLUXCOM GPP together with EC GPP data at de different FLUXNET EC towers.

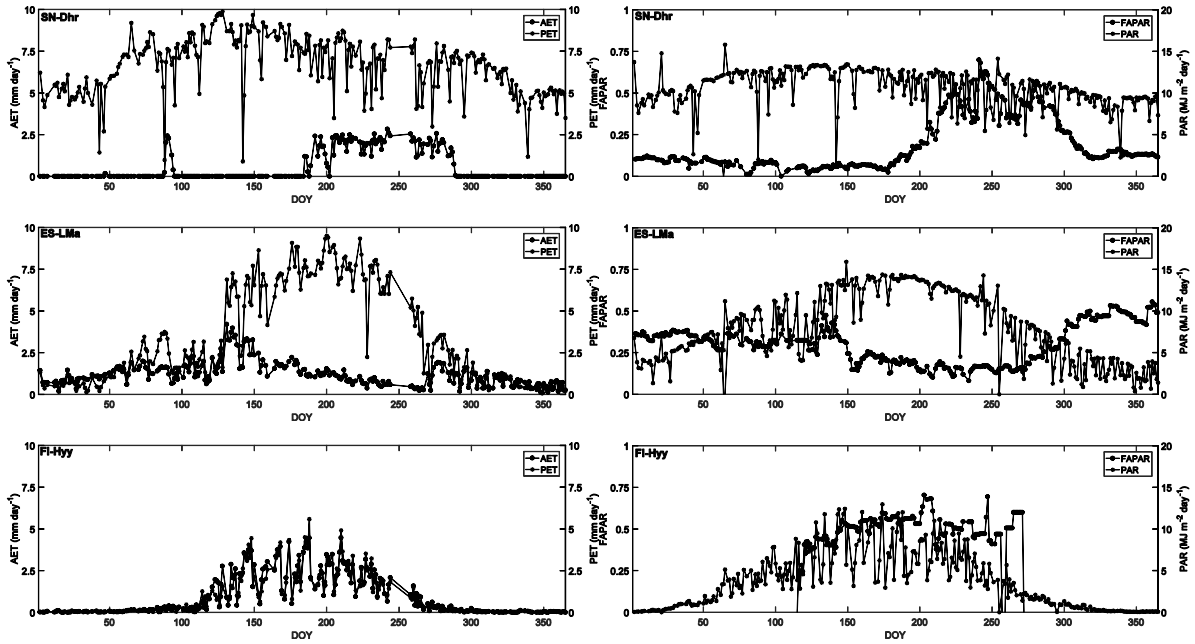


**Figure 4.** Temporal variation of AET and PET (left) as well as  $f_{APAR}$  and PAR (right) for two sites with water shortage limitations, SN-Dhr (Senegal) and ES-LMa (Spain), and a non-water limited typical forest ecosystem site in Finland, FI-Hyy, for 2012.

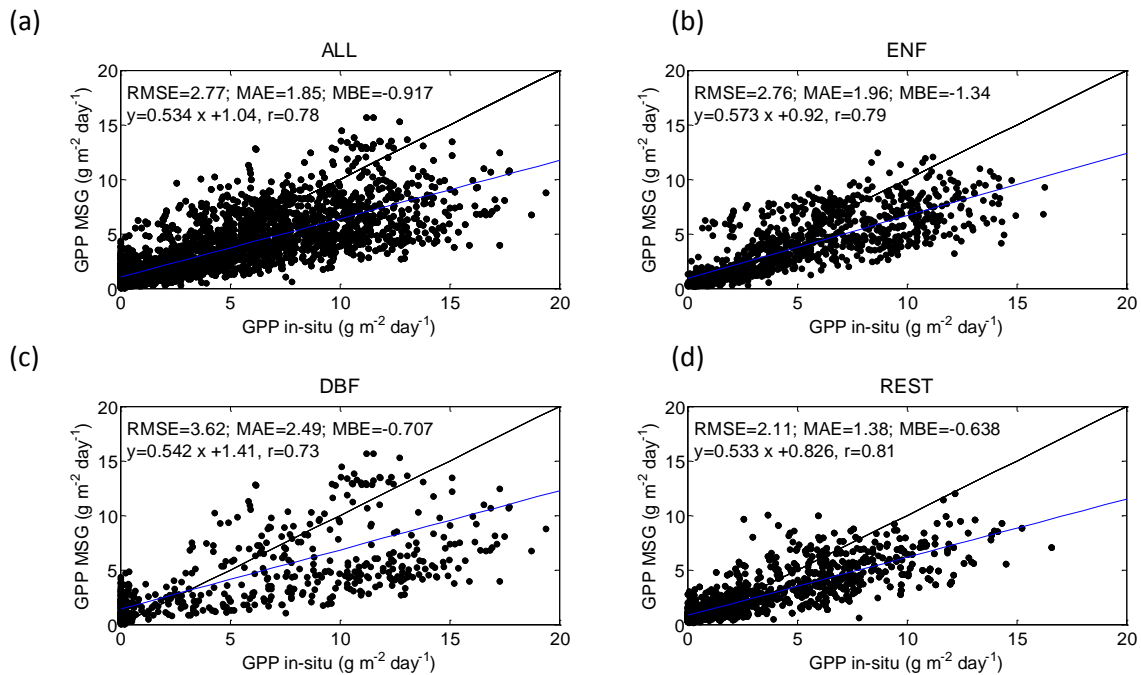


**Figure 5.** Evaluation of the MSG GPP against *in situ* EC GPP for the all the sites (a) and for the sites according to ENF (b), DBF (c) and rest of land covers (d). The black lines show the one-to-one ratios, whereas the blue lines are the fitted ordinary least square regression.

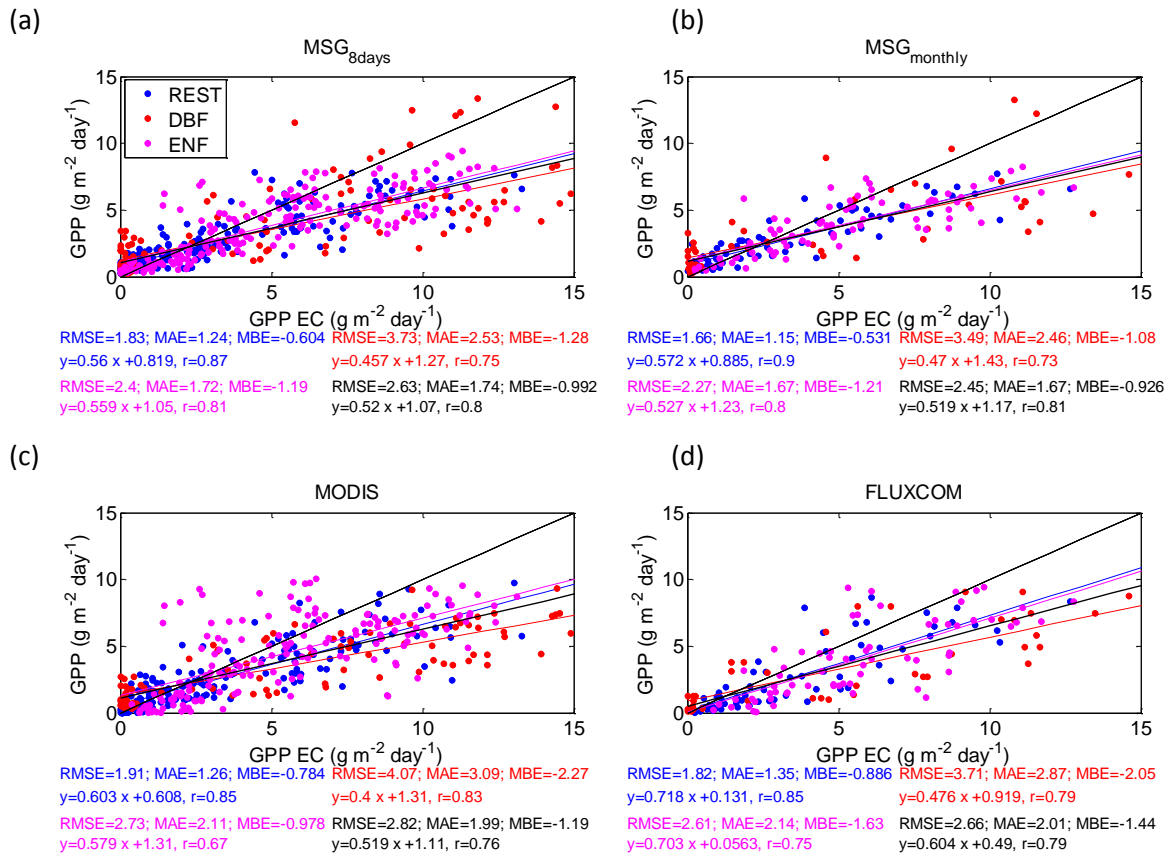


**Figure 6.** MSG GPP re-sampled at 8-day (a) and monthly (b) temporal resolutions against EC GPP values. MSG along with GPP MODIS (c) and GPP FLUXCOM (d) vs. EC GPP are also presented. The RMSE, MAE, MBE, r and linear regression are computed for the ENF (red), DBF (magenta), REST (blue) and ALL (black) sites. The black thin lines show the one-to-one ratios. The thick black lines show the fitted ordinary least square regression when all sites are considering. The red, magenta and blue lines show the fitted ordinary least square regression for the ENF, DBF and REST flux towers.

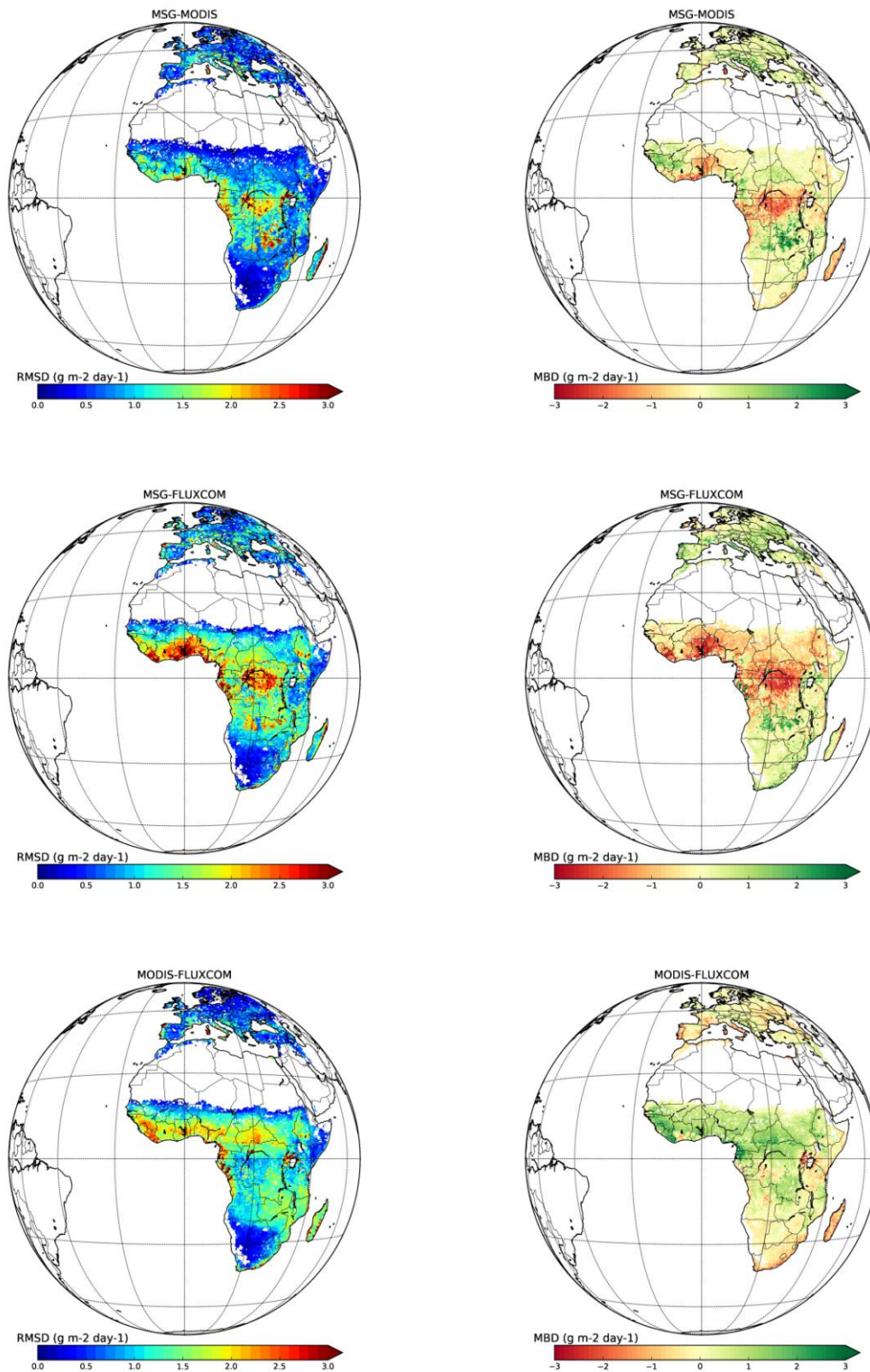


**Figure 7.** RMSD and MBD (in  $\text{g m}^{-2} \text{ day}^{-1}$ ) between MSG-MODIS (top), MSG-FLUXCOM (centre) and MODIS-FLUXCOM (bottom).

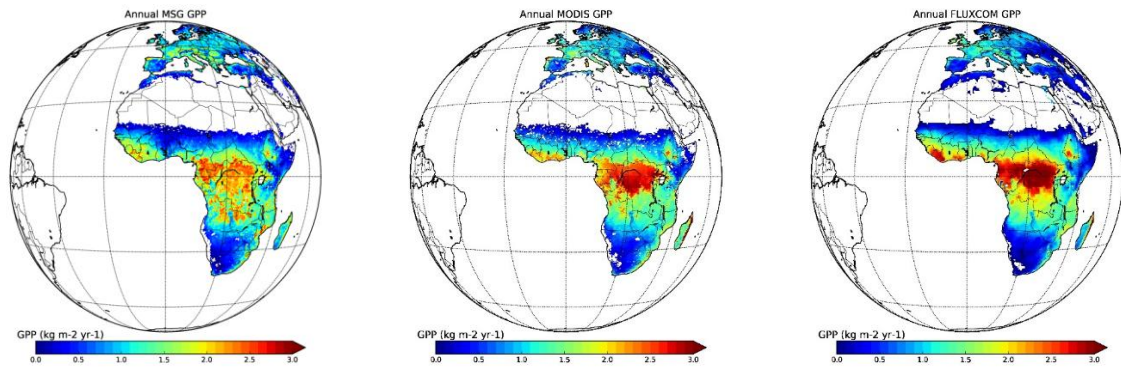


**Figure 8.** Annual GPP estimates for MSG, MODIS and FLUXCOM.

**Supplementary material\***

\*This material has been prepared to show the Jensen and Haise (1965) method applicability over different sites with different PAR and T values.

Two sites, a semi-arid savanna grassland in Africa (SN-Dhr) and a boreal Forest in Finland (FI-Hyy) have hereafter been selected to assess the applicability of the Jensen & Haise model due to Rg and T variability (see Figure below). Both sites are also included in the example of Figure 4 (see manuscript) where the differences in the temporal variation of AET and PET (left) as well as  $f_{APAR}$  and PAR (right) due to water shortage limitations in Senegal and non-water limited typical forest ecosystem in Finland are assessed. Here, the Dahra site shows a constant and high solar irradiation due to its latitudinal location leading to an almost constant temperature along the year with values reaching the 30°. In this case, the PET derived from Jensen and Haise shows high values with a low variability along the year. The PET is very high because it is hot and dry, but since there is very little water the AET is very low or zero for most of the year. In this case, a minimum value of 0.6 is obtained for the  $C_{ws}$  which indicates that photosynthesis is reduced to 60% of its potential due to water shortage reduction. For FI-Hyy, no water limitation is observed and the PET and AET are almost the same along the year. The PET estimates from Jensen and Haise reaches very low values and almost zero when there is very low solar irradiation (winter and autumn seasons) and the air temperature is almost zero or below zero. In this case, the solar irradiation and air temperature are not high enough to convert the water content into vapor and transfer it to the atmosphere. The  $C_{ws}$  is set to 1 (no water stress when the air temperature is below -3.2) since the vegetation canopy is supposed not to be affected by water stress.

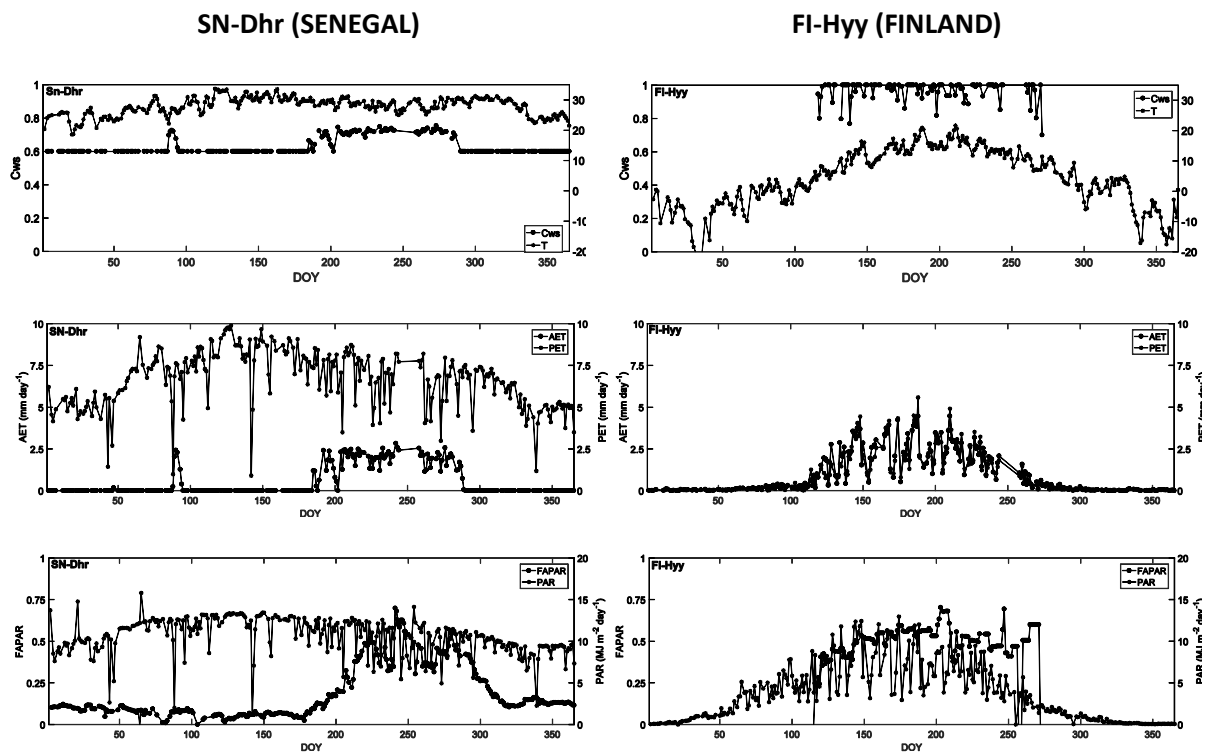


Figure 1. Example for SN-Dhr and FI-Hyy sites.